DISPLACEMENTS OF SUBSTRATE ATOMS INDUCED BY ALKALI-METAL DEPOSITION

アルカリ金属蒸着によって誘起される基板原子の移動

水野　清義

(1)

DISPLACEMENTS OF SUBSTRATE ATOMS INDUCED BY ALKALI-METAL DEPOSITION

アルカリ金属蒸着によって誘起される基板原子の移動

水野　清義

ACKNOWLEDGEMENTS

I would like to express my sincere gratitude to Prof. Hiroshi Tochihara for his guidance and kind advice.

I would like to express appreciation to Prof. Takaaki Kawamura for arrangement of LEED programs and for fruitful discussions.

I would like to thank Prof. Yoshitada Murata, Prof. Kazunobu Hayakawa, Prof. Ken-ichi Tanaka and Prof. Isamu Toyoshima for encouragement.

I also would like to acknowledge Mr. Tadahiko Matsudaira and members in equipment development room for their technical support.

Finally, I would like to thank all the other members in Catalysis Research Center for their encouragement.

ABSTRACT OF THE THESIS

The 2x1, 3x3 and 4x4 patterns of low energy electron diffraction (LEED) have been observed for Li deposition on Cu(001) at room temperature with increase of Li coverage (Chapter II). These patterns are completely different from those of overlayers formed at low temperatures and are considered to be due to displacements of substrate atoms. This proposal is based on the following experimental facts; (1) Thermal activation is required to form the 2x1, 3x3 and 4x4 structures, (2) Unsaturation of intensity of Li interatomic Auger transition termed Li(1s)Cu(3d)Cu(3d) with respect to Li coverage, and (3) Peculiar periodicities of 2x1, 3x3 and 4x4.

In this thesis I focus on displacement of substrate and adsorbate atoms induced by alkali-metal deposition. In order to determine surface structures, we use LEED analysis. For this we need to measure intensity–energy, $I(E)$, curves to compare theoretical calculations obtained from assumed structures. As an approximate method we worked out "Horizontal-beam method" (Chapter III). This method is very useful to reduce the effects of beam-misalignment and to obtain reproducible $I(E)$ curves quickly. First, the c(2x2) structure formed on Cu(001) by Li adsorption at 180 K has been successfully determined by using this method (Chapter IV) . In the calculation we used a program of dynamical LEED intensity calculation.

Then, the 2x1 structure is also successfully determined by means of Horizontal-beam method (Chapter V). The result indicates that the missing-row type restructuring of Cu(001) surface is preferred. This is the first structure determination of the 2x1 structure formed on the fcc(001) surface induced by alkali-metal deposition. Li adatoms replace Cu atoms at every second row in the top layer of Cu(001), and the 2x1 missing-row structure is completed at Li coverge of 0.4.

Furthermore, we try to study behaviors of Li adatom at very low coverages (Chapter VI). We used angle-resolved photoelectron spectroscopy (ARUPS) to get coordination number or removal number of a single Li adatom on Cu(001). The Tamm-type surface state of Cu(001) at $\overline{M}$ point has been monitored as a function of Li coverage at 180 and 300 K. From the slope of attenuation of its intensity we obtained the coodination numbers of a Li adatom at two temperatures. The results are in good agreement with the structures at higher coverages.

The alkali-metal deposition on dissimilar alkali-metal preadsorbed surfaces is also interesting from standpoint of adsorbate displacements (Chapter VII). AES of Li KVV and Na LVV have been used to distinguish whether the alkali-metal atoms sitting on the Cu substrate or locating on the alkali-metal atoms. Simple overlayer formation, substitution, and compression and phase separation are observed for different combinations of alkali-metal atoms.

We have observed various types of displacements of substrate and adsorbate atoms induced by alkali-metal deposition. These displacements were studied by using LEED analysis, ARUPS and interatomic Auger transitions of alkali-metal atoms. Displacements of substrate or/and adsorbate atoms might play a significant role in various surface processes and phenomena such as diffusion, ordering, phase transition, surface materials formation, catalysis and so on.

CONTENTS

I. General Introduction

One of the most important results of this thesis is a structure determination of a Li/Cu(001)-2x1 system as a missing-row type restructuring. It has been believed that the alkali-metals make hexagonal-like overlayer and prefer the hollow site on the metal surfaces except some special cases. However, quite recently, a lot of exceptions are discovered. Substitution, intermixing and adsorption onto the on-top site really occur on metal surfaces under alkali-metal deposition. These surface structures are determined by low energy electron diffraction (LEED) analysis, surface extended X-ray-absorption fine-structure (SEXAFS) and normal incidence standing X-ray wavefield absorption (NISXW). Since these unusual adsorptions occur even at room temperature, the structure should be studied first. Moreover, since these structures are very novel, the structures should be clarified by using structure determination techniques before the origin of unusual structure formations is discussed. To accomplish this purpose, the structure of Li/Cu(001)-2x1 has been determined by *I(E)* analysis of LEED as described in chapter V.

In this thesis, it is demonstrated that the ability of Auger electron spectroscopy (AES) as well as LEED. The AES is able to distinguish whether alkali-metals make bonding with Cu or not, as described in chapters II, VII and VIII. It means that it is possible to distinguish between first-layer and second-layer of alkali-metals when alkali-metals form overlayers. Moreover, it is able to determine mixing ratios of alkali-metal and Cu substrate atoms in the topmost layer when they form intermixed surface alloy. Such information is very useful to make models for surface structures.

1. Usual alkali-metal adsorption

The alkali-metal adsorptions have been studied for many years [1]. A lot of overlayer structures have been observed by LEED. Because the bond strength of alkali-metal to substrate is larger than that of alkali-metals themselves, alkali-metal adatoms form overlayer with layer-by-layer growth. In monolayer region, the overlayer structure changes with the coverage of alkali-metals. These structure changes are explained by two competitive factors. One is the repulsion between alkali-metal atoms because they have dipole moment pointing to the surface normal. The other is the surface corrugation of the substrate. The case of fcc(001) surface, the fourfold hollow site seems most suitable site. Müller *et al.* has been reviewed the series of structure changes for many systems [2].

We have studied K, Na and Li adsorption onto Cu(001) at low temperature. Structures in monolayer region are explained by overlayer models. At low temperature (180 K) alkali-metal atoms cannot substitute the substrate Cu atoms. However, alkali-metal atoms can move arround on the Cu surface. For instance, for the case of Li on Cu(001), the c(2x2) pattern is observed at Li coverage of 0.2, although the local coverage of the c(2x2) is 0.5 [3]. If Li atoms cannot move arround, it is not able to explain why the c(2x2) structure appears at lower coverages. Island formation at low coverages are also found on Al(111) surface [4]. These results also indicate an attractive interaction between alkali-metal atoms [5].

2. Alkali-metal induced reconstruction of fcc(110) surfaces

The fcc(110) surface is the special case of alkali-metal adsorption. Even at the clean surface, some kind of metals reconstruct to 1x2. This structure is determined to be a missing-row type reconstruction. From the structural feature, this type of reconstruction is reasonable. Therefore, alkali-metal induced reconstruction is also probable. However, the missing-row model was doubted because half of topmost substrate layer have to vanish. It was not

believed that the substrate atoms move around on the surface very easily at room temperature. From this reason, other models are considered; saw-tooth and paired-row models. However, the missing-row model is proved by LEED and other tecniques for alkali-metal covered surfaces [6]. This means that the substrate atoms can move arround even at room temperature under alkali-metal deposition.

Next, the mechanism of the alkali-metal induced missing-row type reconstruction was discussed. The electron donation from alkali-metal to substrate was considered, because the 1x2 structure is observed at relatively low coverages by LEED. However, Schuster *et al.* have shown the local reconstruction for the K/Cu(110) system by using STM [7]. The cavities which is occupied by K atoms can move very easily even at room temperature. With increasing K coverage, the cavities align each other and make 1x4 and 1x3 periodicities. Finally it makes ordered 1x2 missing-row structure at coverage of 0.2.

3. Unusual alkali-metal adsorption

The 2x1 restructuring of fcc(001) surface is discovered by Okada *et al.* for the K/Ag(001) system and this is assigned missing-row type restructuring [8]. In case of fcc(001) surface, however, it is not natural to make missing-rows. Because the fcc(001) surface has a square unit cell, there is no reason to make missing-rows which are alingned to one direction. Nevertheless, the 2x1 reconstructions are also found for Li/Cu(001) [3] and K/Au(001) [9,10] systems and these are also assigned as the missing-row type restructuring. At higher coverages of Li/Cu(001) system, 3x3 and 4x4 structures are found and these are assigned as surface alloys.

At that time, unusual adsorptions on fcc(111) surface are reported. Na/Al(111) and K/Al(111) systems are typical cases [11-14]. At low temperature, K atom adsorbs onto on-top site. At room temperature, K atom

substitutes the Al substrate atoms. Na atom also substitutes the Al substrate atoms at room temperature. Moreover, Na makes intermixed layers with substrate at higher coverages. These structures are determined by using SEXAFS, LEED and NISXW.

Nakanishi *et al.* have been observed nx1 structures for the Li/Cu(110) system [15]. These stuructures are assingned surface alloys. This means that the unusual alkali-metal adsorption is not limited by surface plane.

4. Necessity of structure determination

From LEED patterns, we only know the surface periodicities. We cannot determine adsorption sites and arrangement of different elements which causes the surface periodicity. At low temperatures, alkali-metals form overlayers. Therefore, adsorption sites should be determined. It was believed that alkali-metals adsorb onto the hollow site because the hollow site has the highest coordination number. This picture is realized for fcc(001) surface. The adsorption onto fourfold hollow sites is determined for Li/Cu(001) [16], Na/Al(001) [17] and K/Ni(001) [18] systems. Then, it should be expected that the threefold hollow site is the best adsorption site for fcc(111) surface. However the on-top site adsorption is found for some systems as described above. Even if alkali-atoms adsorb on threefold hollow site of hexagonal packed surface, there are two possible sites. For the K/Ru(0001) system, the adsorption site of K is altered with coverages from fcc site to hcp site [19]. These results clearly demonstrate the necessity of the structure determination.

At room temperature, the situation is more complex because not only alkali-metals but also substrate atoms can move around. There is too much possibilities to conclude a structure without structure determination techniques. The structure determination is conclusively necessary.

Nevertheless, it is also important to make good models in advance before structure determination. For this purpose, some indirect methods are

important. For Li/Cu(001)-2x1, streaky spots appear in the LEED pattern [3]. From the behavior of the streaky spots, it is able to make reasonable models. AES is also useful to determine coverages and is possible to find the growth mode, as described in chapter VII.

References

[1] H. P. Bonzel, A. M. Bradshaw and G. Ertl, Eds., Physics and Chemistry of Alkali Metal Adsorption (Elsevier, Amsterdam, 1989).

[2] K. Müller, G. Besold and K. Heinz, in ref. [1], p. 65.

[3] H. Tochihara and S. Mizuno, Surf. Sci. **279**, 89 (1992).

[4] M. Scheffler, Ch. Droste, A. F. Leazar, F. Maca, G. Wachutka and G. Barzel, Physica **B172**, 143 (1991).

[5] J. Neugebauer and M. Scheffler, Phys. Rev. Lett. **71**, 577 (1993).

[6] R.J. Behm, in ref. [1], p. 111.

[7] R. Schuster, J.V. Barth, G. Ertl and R.J. Behm, Surf. Sci. **247** (1991) L229; Phys. Rev. **B44** (1991) 13689.

[8] M. Okada, H.Tochihara and Y. Murata, Phys. Rev. B43 (1991) 1411; Surf. Sci. **245** (1991) 380.

[9] M. Okada, H. Iwai, R. Klauser and Y. Murata, J. Phys.: Condens. Matter **4** (1992) L593.

[10] J.V. Barth, R. Shuster, R.J. Behm and G. Ertl, Surf. Sci. **302** (1994) 158.

[11] A. Schmalz, S. Aminpirooz, L. Becker, J. Haase, J. Neugebauer, M. Scheffler, D.R. Batchelor, D.L. Adams and E. Bøgh, Phys. Rev. Lett. **67** (1991) 2163.

[12] J.N. Andersen, M. Qvarford, R. Nyholm, J.F. van Acker and E. Lundgren, Phys. Rev. Lett. **68** (1992) 94.

[13] C. Stampfl, M. Scheffler, H. Over, J. Burchhardt, M. Nielsen, D.L. Adams and W. Moritz, Phys. Rev. Lett. **69** (1992) 1532.

[14] M. Kerkar, D. Fisher, D.P. Woodruff, R.G. Jones, R.D. Diehl and B. Cowie, Surf. Sci. **278** (1992) 246.

[15] S. Nakanishi, T. Yumura, K. Umezawa, H. Tochihara and S. Mizuno, Phys. Rev. **B49**, 4850 (1994).

[16] S. Mizuno, H. Tochihara and T. Kawamura, Surf. Sci. **293**, 239 (1993).

[17] B.A. Hutchins, T.N. Rhodin and J.E. Demuth, Surf. Sci. **54**, 419 (1976).

[18] U. Muschiol, P. Bayer, K. Heinz, W. Oed and J.B. Pendry, Surf. Sci. **275**, 185 (1992).

[19] M. Gierer, H. Bludau, T. Hertel, H. Over, W. Moritz and G. Ertl, Surf. Sci. **279** (1992) L170.

II. Observation of anomalous LEED patterns from Li adsorbed Cu(001): 2x1, 3x3 and 4x4

Lithium adsorption on Cu(001) at 300 K has been studied with low-energy electron diffraction (LEED) and Auger electron spectroscopy. LEED patterns show a sequential change with increasing Li coverage; 2x1, 3x3 and 4x4. The 2x1 LEED pattern accompanies weak streaky spots denoted by a matrix of $\begin{pmatrix} \frac{1}{2}\Theta & 0 \\ -\frac{1}{4}\Theta & 2 \end{pmatrix}$ in a coverage range of $0.375 \leq \Theta \leq 0.4$. The 4x4 pattern disappears with further Li deposition and the surface becomes disorder. Features and behaviors of the streaky spots are very similar to those observed for systems of K or Cs adsorption on Ni(110) or Cu(110) at room temperature, and this leads to a structure model for 2x1; the Cu(001) surface undergoes missing row type restructuring induced by Li adsorption. Li adatoms are located in missing rows formed by themselves and result in exhibiting the streaky spots. Possible structure models for the 3x3 and 4x4 structures are proposed and they are assigned to ordered surface-alloys of LiCu on Cu(001).

1. Introduction

Various ordered structures of alkali metal (AM) overlayers are developed during monolayer formation on metal surfaces [1]. In particular, it is interesting to study the adsorption of AM atoms on fcc(001) metal surfaces for understanding AM overlayer structures, because we can easily distinguish structures of the AM overlayers from that of the substrate in low-energy electron diffraction (LEED) patterns [2]. That is, usually structures of AM overlayers are quasihexagonals resulting from two competing interactions; an interaction of AM adatoms with a square lattice of the substrate and an interaction between AM adatoms. However, Okada et al. have recently

observed, for the first time, non-quasihexagonal structures in LEED patterns for K/Ag(001) at 315-335 K; 2x1 and 3x1 [3]. These anisotropic patterns have been attributed to reconstructions of the substrate surface induced by K adatoms.

On the other hand, it is well known that AM adatoms induce reconstructions of missing row type on fcc(110) metal surfaces such as Ni, Pd, Cu and Ag at room temperature [4-8]. Recent STM studies by Schuster *et al.* for K/Cu(110) have demonstrated that a single K atom removes the substrate metal atoms and thus created vacancies in the top layer of Cu(110) grow as missing rows with increasing K coverage [4]. Although the detailed mechanism of this AM induced reconstruction is still in debate [9,10], it has become clear that the AM adsorption does not always result in the overlayer formation.

Even on fcc(111), considered to be the most stable surface, very recently Schmalz *et al.* have found that Na adatoms substitute surface Al atoms on Al(111) to form a $(\sqrt{3}x\sqrt{3})R30°$ structure at room temperature from surface extended X-ray-absorption fine-structure measurements [11]. Furthermore, Andersen *et al.* have studied the same adsorption system at room temperature with a high-resolution core-level spectroscopy and they have concluded that 2x2 and $2\sqrt{3}x2\sqrt{3}$ structures observed at higher coverages consist of intermixed Na-Al layers [12].

As briefly reviewed above, the AM adsorption on metal surfaces seems to be rich in variety. In this chapter, LEED observations for Li/Cu(001) at 300 K are reported. Three ordered structures, 2x1, 3x3 and 4x4, have been found with increasing Li coverage. Weak streaky spots are coexisting in the 2x1 pattern. As mentioned above, the 2x1 pattern was already observed for K/Ag(001) [3], but the 3x3 and 4x4 patterns have not been observed so far for AM atom adsorption on fcc(001) metal surfaces. Possible structural models for the three superstructures are proposed in this chapter.

2. Experiments

The experiments were carried out in a three-level UHV chamber equipped with various probes [13]. LEED and Auger electron spectroscopy (AES) were principal tools in the present study. A rearview LEED optics (Omicron) was used to monitor surface structures. AES in a derivative mode was measured for lithium *KVV* using an analyzer for X-ray photoelectron spectroscopy (XPS) with a 600 eV incident electron energy. After mechanical polishing to a mirror finish, a Cu(001) specimen was electrolytically polished in a solution of HNO_3 and CH_3OH at 220 K. The sample was rectangular shape of 7x11x1.5 mm^3 and held on a Ta holder with thin Cu wires through small holes spark-drilled at its corners. After an argon ion sputtering (5$\mu A/cm^2$, 500eV) for 10 min at 300 K, the sample was annealed up to 750 K by an electron beam heater behind the holder. Surface cleanliness was confirmed by AES and XPS. LEED spots were sharp and the background was satisfactorily low. Li was deposited onto the surface from a SAES dispenser (SAES Getters). During Li deposition the pressure was less than $1.5x10^{-10}$ Torr. Only water in the chamber was adsorbed on the Li covered Cu surface at 300 K and its partial pressure was less than $1x10^{-11}$ Torr [13,14].

3. Results

3.1. LEED observations

In Fig. 1, sequential changes of LEED patterns observed at 300 and 180 K are summarized as a function of Li coverage, θ. How to determine θ will be mentioned below. θ=1 corresponds to 1 Li atom per 1 Cu atom in the ideal topmost surface. At 180 K, a superstructure observed first is c(2x2), then LEED pattern changes successively to structures denoted by matrices with increasing coverage [15]. At 300 K LEED exhibits completely different superstructures; 2x1, 3x3, then 4x4. The 2x1 pattern is accompanied with

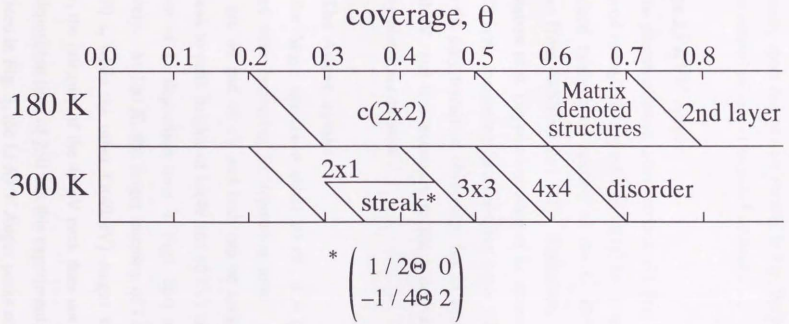

Fig. 1. Surface-structure changes for Li/Cu(001) at 180 K and 300 K as a function of Li coverage,θ. A matrix notation of streaky spots observed at 300 K is shown at bottom. See text for the meaning of Θ.

weak streaky spots shifting as a function of θ. The 4x4 pattern disappears rather quickly with an additional Li deposition, then the surface becomes disorder. In Fig. 2, LEED pictures of 2x1, 3x3 and 4x4 are shown. The weak streaky spots can be seen clearly in Fig. 2(a), where both the streaky and 2x1 spots consist of two orthogonal domains.

3.2. The Li *KVV* Auger

Since photoionization cross sections of Li(1s) is so small, it is difficult to obtain good enough XPS spectra of Li(1s) for a monolayer range. Previously we obtained fairly good spectra of the Li *KVV* Auger in submonolayer coverages from Li/Si(001)2x1 [16]. Therefore, we employed AES for the determination of θ. The concentration of Li adatoms on Cu(001) is monitored with AES with increasing Li deposition time. The *KVV* Auger transition, which is the only transition observable for Li adatoms, should be observed at about 50 eV, and it is necessary to use a derivative mode to avoid intense secondary electron emission.

3.2.1. The Auger uptake

In the Auger spectra at about 50 eV, it is found that two features are developed with increasing Li deposition time. Peak positions of the two features are 46 and 49 eV and both can be assigned to the Li Auger. The Auger peak-to-peak heights of Li(49 and 46 eV) and Cu(60 eV) are plotted as a function of Li deposition time in Figs. 3(a) and (b) at 180 and 300 K, respectively. At 180 K, the Auger intensity of Li(46 eV) stops increasing at about 150 s, while the other Li(49 eV) Auger keeps on growing. On the contrary, the intensity of the 46 eV peak does not saturate at 300 K up to the longest deposition time of 250 s in this experiment.

As seen in Fig. 3, the Li *KVV* Auger peaks could not be detected up to 40 s, probably because the Auger signal is hidden by the intense background from

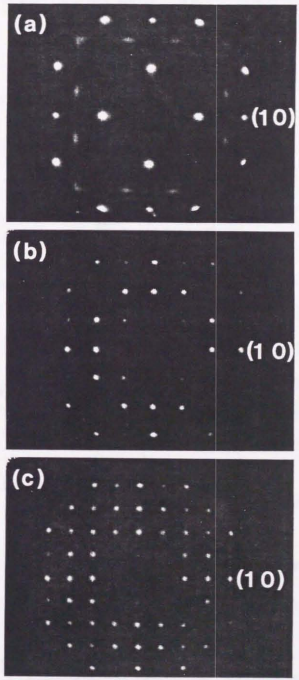

Fig. 2. LEED pictures of the Li/Cu(001) system at 300 K for (a) 2x1 at 50 eV, (b) 3x3 at 60 eV and (c) 4x4 at 53 eV. The (1 0) spots are indicated.

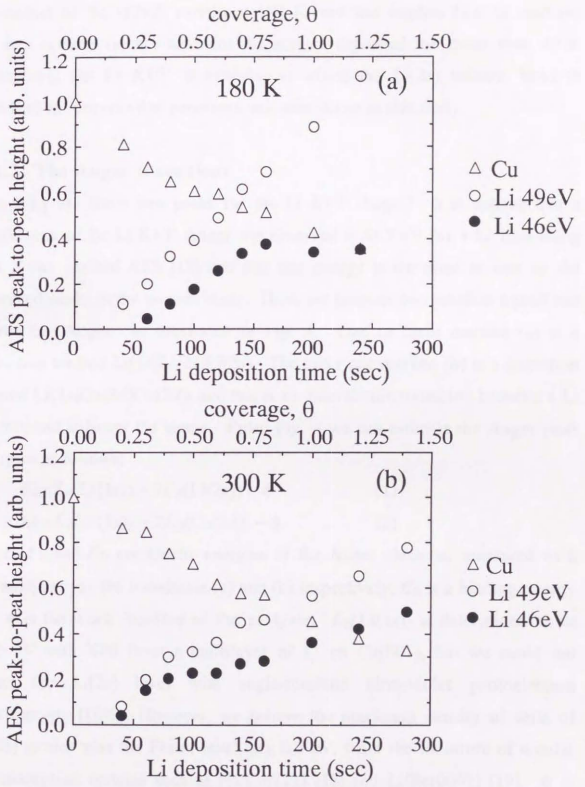

Fig. 3. Auger peak heights of Li (49 and 46 eV) and Cu (60 eV) versus Li deposition time (a) at 180 K and (b) at 300 K. Li coverage, θ, is also shown.

the Cu substrate. Li deposition time of 40 s corresponds to the initial formation of the c(2x2) pattern at 180 K, and this implies that Li adatoms form a surface valence-band for the surface deposited for more than 40 s. Therefore, the Li *KVV* transitions, in which the Li(2s) valence band is involved in deexcitation processes, are considered in this study.

3.2.2. The Auger transitions

Why are there two peaks for the Li *KVV* Auger? It is noticed that a single peak of the Li *KVV* Auger was observed at 48.7 eV for a Li film using soft X-ray excited AES [17] and that this energy is the same as one of the observed peaks in the present study. Here, we propose two possible transitions of the Li Auger as illustrated in Fig. 4. One of them marked (a) is a transition termed Li(1*s*)Li(2*s*)Li(2*s*). The other one marked (b) is a transition termed Li(1*s*)Cu(3*d*)Cu(3*d*), and this is an interatomic transition between a Li adatom and adjacent Cu atoms. From Fig. 4 we can estimate the Auger peak energies as follows:

$$E_a = E_B(\mathrm{Li}(1s)) - 2E_B(\mathrm{Li}(2s)) - \phi \qquad (1)$$

$$E_b = E_B(\mathrm{Li}(1s)) - 2E_B(\mathrm{Cu}(3d)) - \phi, \qquad (2)$$

where E_a and E_b are kinetic energies of the Auger electrons measured with the analyzer for the transitions (a) and (b) respectively, E_B is a binding energy and ϕ is the work function of the analyzer. E_B(Li(1*s*)) is determined to be 54.8 eV with XPS from a multilayer of Li on Cu(001), but we could not detect the Li(2*s*) level with angle-resolved ultra-violet photoelectron spectroscopy (UPS). However, we believe the maximum density of state of Li(2*s*) locates near the Fermi level, say 0.2 eV, from the literature of similar chemisorption systems such as Na/Cu(111) [18] and Li/Be(0001) [19]. ϕ is determined to be 5.1 eV from XPS of Cu($2p_{3/2}$) at 932.4 eV. From these data and equation (1), the Li(1*s*)Li(2*s*)Li(2*s*) transition peak will appear at 49.3 eV. This is in good agreement with our result, 49 eV. On the other hand, the

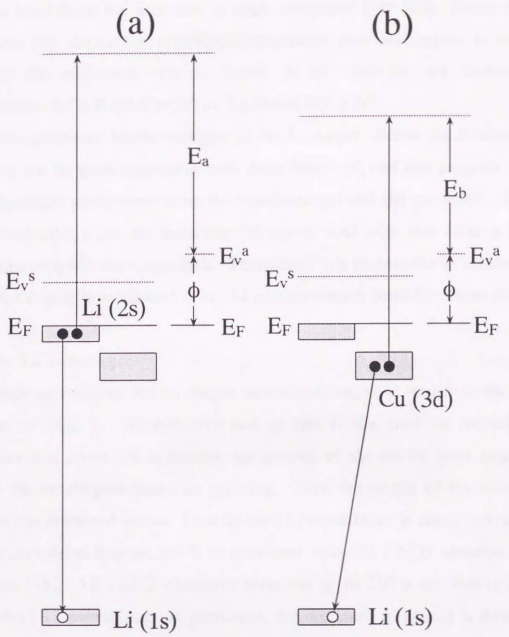

Fig. 4. Two possible transitions of the Li KVV Auger; (a) Li(1s)Li(2s)Li(2s) transition and (b) Li(1s)Cu(3d)Cu(3d) transition. E_F is the Fermi level. E_V^s and E_V^a are the vacuum levels for the sample and analyzer, respectively. ϕ is the work function of the analyzer. E_a and E_b are kinetic energies measured by the analyzer for transitions (a) and (b), respectively.

maximum density of state of the Cu(3*d*) band locates at 2.2 eV below the Fermi level from the literature of angle integrated UPS [20]. From this and equation (2), the Li(1*s*)Cu(3*d*)Cu(3*d*) transition peak will appear at 45.3 eV. This is also consistent with our result, 46 eV. We did not observe cross transitions; Li(1*s*)Li(2*s*)Cu(3*d*) or Li(1*s*)Cu(3*d*)Li(2*s*).

The predicted kinetic energies of the Li Auger due to the transitions (a) and (b) are in good agreement with those observed, and this suggests that the two Li Auger peaks come from the transitions (a) and (b) proposed. That the observed energy for the transition (a) agrees well with that from a Li film [17] also supports the assignment. Therefore, it is reasonable to conclude that the 46 eV peak is originated from Li adatoms which bond Cu atoms directly.

3.2.3. Li coverages

Having assigned the Li Auger transitions, we now return to the uptake curves of Fig. 3. We conclude that at 180 K the first Li monolayer is completed at about 150 s, because the growth of the 46 eV peak stops there while the 49 eV peak keeps on growing. Note the origin of the two Auger transitions discussed above. That the first Li-monolayer is completed at about 150 s deposition time at 180 K is consistent with the LEED observation and analysis [15]. All LEED structures observed up to 150 s are explained with models of Li overlayers. In particular, the structure of c(2x2) is determined with the LEED intensity analysis and it is found that the c(2x2) structure is caused by Li adatoms on hollow sites of Cu(001) [21]. Further details will be described in Chapter IV. Therefore, we conclude that θ is 0.5 for the surface which indicates the maximum spot-intensity of c(2x2) at 180 K.

On the other hand, the Auger uptake of the Li(46 eV) peak at 300 K is quite different from that at 180 K, as shown in Fig. 3(b). The intensity of the Li(46 eV) Auger does not indicate saturation at 150 s but increases monotonically. There is no distinct break-point indicating the first

monolayer. Therefore, it is difficult to determine θ at 300 K. We assume that sticking coefficients of Li on the surfaces at 180 and 300 K are the same, then we can obtain θ at 300 K by using deposition time. This assumption seems to be a good approximation at least at low θ (θ < 0.7) as mentioned below.

Thus obtained coverages are used in Fig. 1. Slashes are employed to separate neighboring structures in Fig. 1, because an error in θ is estimated to be 0.1 owing to discontinuous Li depositions in the present study. The assumption for the sticking coefficient above seems to be correct, because we have confirmed that a structure formed at 180 K changes to a corresponding structure having the same coverage at 300 K when annealed. That is, the c(2x2) and matrix-denoted structures prepared separately at 180 K were converted to the 3x3 structure (the 2x1 structure is also formed when θ is lower) and a disordered structure respectively when the sample was annealed to 300 K (see Fig. 1). Therefore, we are sure that Fig. 1 summarizes changes of structures for Li/Cu(001) at 180 and 300 K as a function of θ.

3.3. The streaky spots

At the bottom of Fig. 1, a matrix notation $\begin{pmatrix} \frac{1}{2}\Theta & 0 \\ -\frac{1}{4}\Theta & 2 \end{pmatrix}$ for the streaky spots is shown, in which it should be noticed that Θ is used instead of θ. Θ is a kind of local coverage derived from LEED pictures, while θ is a coverage averaged over a wide area illuminated by an electron beam. Here, we examine features of the streaky spots in detail. Fig. 5 shows a schematic illustration of the streaky spots (elliptic shape) with the 2x1 spots. There are two orthogonal-domains for both the 2x1 and streaky structures, but for simplicity only one of them is depicted with unit meshes in Fig. 5 . The 2x1 and streaky spots belonging to the same domain (see Fig. 5) could be distinguished, when we prepared a nearly single-domain surface accidentally. As mentioned above, the streaky spots shift with increasing θ, and this shift is indicated by arrows in

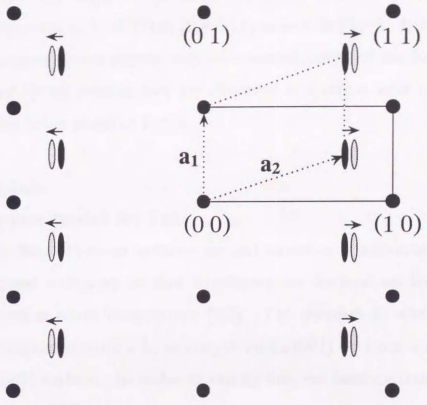

Fig. 5. A schematic illustration of a normal incident LEED pattern consisting of the 2x1 and streaky spots. See the LEED picture of Fig. 2(a). For simplicity, a single domain for both structures is depicted and the streaky shape is not depicted for spots which belong also to the 2x1 spots. Unit meshes for the 2x1 and streaky spots are shown with solid and dotted lines, respectively. $\mathbf{a}_1$ and $\mathbf{a}_2$ are the basis vectors of the streaky spots in the LEED pattern. Solid and dotted ellipses correspond to the first and last streaky spots observed with increasing Li deposition time, respectively. Arrows indicate the shift of the streaky spots with increasing Li coverage. See text in detail.

Fig. 5. The solid and dotted ellipses correspond to the first and last streaky spots observed with increasing θ, and their local coverages, Θ, deduced from the LEED pictures are 0.375 and 0.4, respectively. During the shift while one basis vector, $\mathbf{a}_1$, stays at (0 0.5), the other basis vector, $\mathbf{a}_2$, moves continuously from (0.75 0.25) to (0.8 0.25) as seen in Fig. 5. It is noticed that the streaky spots would appear only in a limited range of the local coverage ($0.375 \leq \Theta \leq 0.4$) but actually they are observed in a rather wide range of θ as shown in the lower panel of Fig. 1.

4. Discussion

4.1. Structure model for 2x1

On the fcc(001) metal surfaces, the 2x1 structure is anisotropic. Usually, quasihexagonal structures of AM overlayers are formed on fcc(001) metal surfaces even at room temperature [1,2]. The question is whether the 2x1 pattern is originated from a Li overlayer on Cu(001) or from a restructuring of the Cu(001) surface. In order to clarify this, we have carried out a series of experiment as follows.

First of all, we prepared the c(2x2) structure by Li deposition at 180 K (θ~0.3), then the sample was heated up to 300 K. At about 200 K, LEED changed from the c(2x2) to 2x1 structure. In the 2x1 pattern, the streaky spots coexisted. Next, the sample was cooled down to 180 K, then the streaky spots became distinct spots. LEED exhibited somewhat brighter spots of 2x1, but the c(2x2) pattern did not appear. At 180 K, we dosed Li further on the surface (θ~0.4), then the streaky spots (actually they were spotty) became brighter and shifted similar way as shown in Fig. 5. With further Li deposition (θ~0.5), the 2x1 pattern remained with higher background. Finally, the sample was heated to 300 K, then the 2x1 changed to 3x3 pattern.

This series of experiment clearly demonstrates that a thermal activation is required to form the 2x1 and 3x3 structures. Since the c(2x2) pattern is

observable at θ~0.2 at 180 K (see Fig. 1), Li adatoms can migrate on the Cu(001) surface even at 180 K. Therefore, the thermal activation required is not for the Li adatoms but for the surface Cu atoms. Here, we conclude that the 2x1 structure is not originated from the Li overlayer but is related to a restructuring of the surface Cu atoms. The temperature required for the restructuring is about 200 K, and the restructuring is an activated and irreversible process.

What kind of restructuring is this? Before we go to this point, we pay attention to the streaky spots accompanying the 2x1 structure, because there is a clue for understanding the 2x1 structure. Now we return to Fig. 5, from which we can extract following features of the streaky spots. (1) One basis vector of the unit mesh of the streaky spots, $\mathbf{a}_1$, coincides with one basis vector of that for the 2x1 spots and does not shift as Li coverage increases. (2) The other basis vector, $\mathbf{a}_2$, points (2Θ 0.25) and shifts along the [1 0] direction within a limited range of $0.375 \leq \Theta \leq 0.4$. (3) The streaky spots are elongated parallel to the [0 1] direction but are narrow across the [1 0] direction. In addition to the features above, the experiment mentioned in this chapter provide two characteristic behaviors of the streaky spots. (4) The streaky spots become distinct spots when the sample is cooled down to 180 K. (5) Even at 180 K, the streaky spots shift with Li deposition on the 2x1 structure, and this indicates that the thermal activation is not required for the development of the structure causing the streaky spots while required for the 2x1 formation.

All the features and behaviors of the streaky spots above are very similar to those found for systems of K or Cs on Ni(110) [7] or on Cu(110) [8]. In these studies it has been concluded that distinct spots of the 1x2 pattern are due to the substrate surface reconstruction of missing row type and streaks running along the [0 1] direction are originated from AM adatoms locating in

the missing rows [5-8]. In each missing row AM adatoms are ordered, but between rows there is no correlation due to thermal fluctuation.

The strong similarity of the LEED features between two systems, *i. e.*, Li on Cu(001) and K or Cs on Cu(110) or Ni(110), leads to a following suggestion; the 2x1 structure is due to the restructuring of missing row type on the Cu(001) surface induced by Li adatoms and the streaky spots are originated from the Li atoms sitting in troughs formed by themselves. In Fig. 6(a) the proposed model for the single domain is depicted.

By using this model, we can explain the features and behaviors of the streaky spots mentioned above (from (1) to (5)) naturally as follows. As clearly seen in Fig. 6(a), the structure causing the streaky spots (henceforth we call it *Li chain*) is strongly related with that of 2x1 (henceforth we call it *missing row*). As Li adatoms substitute the Cu surface atoms of every second row, missing rows are formed along, say the [110] direction as shown in Fig. 6(a). It is natural that both *missing row* and *Li chain* structures have the same periodicity along $[\bar{1}10]$, namely, twice of the substrate lattice. The formation of missing rows would be completed first, then the order of Li adatoms would be developed in the troughs. With increasing Li coverage, Li adatoms line up in the troughs with a distance of $(1/2\ \Theta)a$ where a is the nearest-neighbor distance of Cu atoms, and this is the reason why $\mathbf{a}_2$ shifts but $\mathbf{a}_1$ stays with increasing Li coverage. One will understand why the streaky spots appears, when one sees the model of Fig. 6(a). Li adatoms in a trough seem to interact with neighboring Li-chains inefficiently through or over a wall of Cu chain between them, while it seems easier for the Li adatoms to interact each other in the trough. In the present system of Li/Cu(001), there is a short-range order between Li chains, while the disorder between AM chains is prevail at room temperature on the surfaces of K or Cs adsorbed on Ni(110) or Cu(110) probably due to longer spacings between AM chains. We will move on to the next feature. The change from the streaky spots at 300 K to distinct spots at

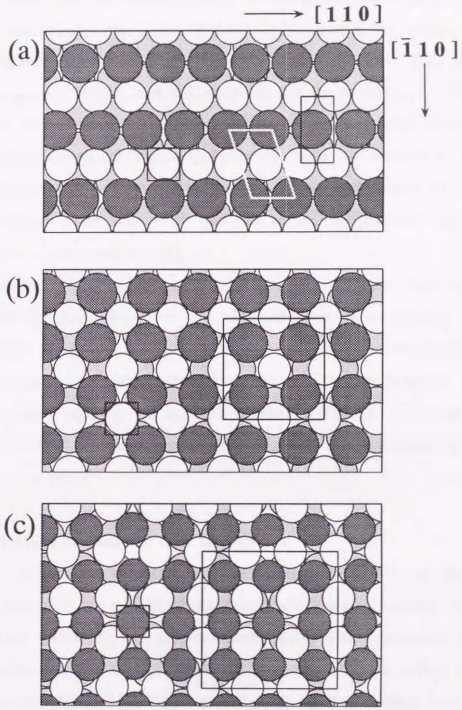

Fig. 6. Top views of structural models of the Li/Cu(001) system for (a) 2x1, (b) 3x3 and(c) 4x4. Black, white and grey circles are Li, Cu in the topmost layer and Cu in the second layer, respectively. In each figure the unit mesh is shown with solid lines together with the 1x1 unit mesh. In (a) Li atoms are ordered to be $\begin{pmatrix} 5/4 & 0 \\ -5/8 & 2 \end{pmatrix}$ and its unit mesh is also outlined with white lines. In (a) and (b) the radius of Li is 1.5 Å (metallic), in (c) this is reduced not to overlap with neighboring Cu atoms.

180 K is also naturally explained with this model; the interaction between Li chains in the troughs overcomes thermal fluctuations at low temperatures and the Li chains undergo a long-range order consequently. This behavior is usually observed in the order-disorder processes at surfaces. Finally, the difference in the thermal activation required for the formation of *missing row* and *Li chain* structures is also understood; while the formation of missing rows is an activated process due to mass transport, development of Li adatoms in the troughs does not need such activation, as generally seen for AM overlayers on metal surfaces [1].

In summary, the 1x2 structure induced on fcc(110) metal surfaces such as Ni and Cu by AM adsorption is established in terms of missing row [4-8]. Therefore, it seems natural that the strong resemblance of the LEED features of the present system with those of fcc(110) leads to a proposal of the similar restructuring of missing row type on fcc(001). The 2x1 structure observed for K/Ag(001) previously was also explained by the restructuring model of missing row type [3].

4.2. Structure model for 3x3 and 4x4

Next, we discuss structures of 3x3 and 4x4. It is obvious that the 3x3 and 4x4 structures are not simple chemisorption systems, because the 3x3 and 4x4 patterns follow the 2x1 pattern successively. The experiment mentioned in the section 4.1. also supports this. That is, the 3x3 pattern does not follow the 2x1 pattern, when Li is dosed at 180 K on the 2x1 surface formed at 300 K. A thermal activation is required to form the 3x3 structure from the 2x1 structure with an additional amount of Li. Both the 3x3 and 4x4 structures are not anisotropic on the fcc(001) surface, and we did not observe any indication of anisotropic features such as streaks in the LEED patterns. Therefore, there is no such a distinct clue for understanding the structures of 3x3 and 4x4 as observed for the 2x1 structure. By using the experimental

facts we try to find models for the 3x3 and 4x4 structures. Then, following conditions should be considered. (1) The 3x3 and 4x4 structures are not due to Li overlayers but involve restructuring of the surface Cu atoms. (2) The 3x3 structure is formed naturally from the 2x1 structure whose structure is shown in Fig. 6(a). (3) The 4x4 structure is formed naturally from the 3x3 structure with increasing Li coverage. (4) The 3x3 and 4x4 structures are formed in limited ranges of Li coverage as suggested from Fig. 1; $0.4<\Theta(3x3)<\Theta(4x4)<0.7$ where $\Theta(3x3)$ and $\Theta(4x4)$ mean Li coverages for models of the 3x3 and 4x4 structures, respectively. From condition (4) and periodicities of 3x3 and 4x4, possible values for $\Theta(3x3)$ and $\Theta(4x4)$ are very limited; 4/9 and 5/9 for $\Theta(3x3)$ and 8/16, 9/16, 10/16 and 11/16 for $\Theta(4x4)$.

We have considered several possible structures satisfying the conditions (1) and (4) above, and finally we have reached quite reasonable models as shown in Figs. 6(b) and (c) for 3x3 and 4x4, respectively. Other structures examined have peculiar arrangements of Li and Cu atoms on the top layer and do not satisfy the conditions (2) and (3). In contrast, the proposed models (Figs. 6(b) and (c)) are very simple and isotropic structures and satisfy the conditions mentioned above. These structures have following features. First, Li and Cu atoms are completely intermixed in the topmost layer on Cu(001). Second, Li and Cu atoms in the top layers of the 3x3 and 4x4 structures form large unit meshes (shown with solid lines in Figs. 6(b) and (c)) which are commensurate with the Cu(001) lattice. Here, we examine how the structure models proposed satisfy the conditions above. To form these surface structures Cu atoms in the top layer of the 2x1 structure have to move, and this satisfies the condition (1). For the condition (4), $\Theta(3x3)$ from this model is 4/9 and this value nicely follow 0.4 of the 2x1 structure. $\Theta(4x4)$ from the model is 9/16 and this also nicely follows 4/9. For the condition (2) it is not unreasonable that the 2x1 structure shown in Fig. 6(a) changes to the 3x3 structure shown in Fig. 6(b) with increasing θ. For the condition (3) if we

approve the model of the 3x3 structure, this model is quite naturally extended to the 4x4 structure. Although the structure models proposed seems to be likely, we are requested to carry out structure determinations by using appropriate techniques.

In the present models the nearest-neighbor distances between Li and Cu in single layers are 2.70 and 2.40 Å for the 3x3 and 4x4 structures respectively, while the sum of metallic radii of Li and Cu is 2.79 Å. Therefore, the model of 3x3 satisfies a metallic bonding scheme between Li and Cu, while the 4x4 model is inconsistent with it. Probably the 4x4 structure is not a single layer but a double layer. The structure models for 3x3 and 4x4 shown in Figs. 6(b) and (c) are quite different from that of 2x1 from a standpoint of the coordination number. A Li atom in the 3x3 and 4x4 structures is coordinated to four Cu atoms in the topmost layer, while a Li atom in the 2x1 structure is coordinated not only to Cu atoms but also to neighboring Li atoms along the trough. The high coordination-number of Li suggests that the 3x3 and 4x4 structures are classified into surface alloys. Since the stoichiometry of Li to Cu is 1:1 for both the 3x3 and 4x4 structures, we denote these surface alloys as LiCu. In fact, Cu and Li form bulk alloys; Li atoms are dissolved into a bulk Cu solid up to 22 % as a solid solution [22].

The ordered 4x4 structure changes to a disordered surface with additional Li deposition, when Li is deposited on the 4x4 structure at 300 K. Probably a formation of a bulk alloy starts, because the Li *KVV* Auger of the 46 eV peak keeps on growing after formation of 4x4 as shown in Fig. 3(b). One should remember that the 46 eV peak reflects the Li adatoms bonding to Cu atoms. Other possibility, *i. e.*, overlayer formation may be excluded, because the 4x4 spots would remain with further Li deposition in that case. Probably, evolving to bulk alloys results in destruction of the ordered surface alloy of the 4x4 structure and formation of a disordered surface.

Finally, it is interesting to note that surface AM alloy formation has been reported recently for Na adsorption on Al(111) by Andersen *et al.* [12] as mentioned at Introduction. They conclude that the 2x2 and $2\sqrt{3}x2\sqrt{3}$ structures at high coverages consist of intermixed Na-Al layers, but it is not clear that these are single layer alloys. Another possible surface AM alloy is a c(2x2) structure observed for K adsorption on Au(110) at room temperature by Häberle and Gustafsson using medium-energy ion scattering analysis [23]. They mentioned that the c(2x2) structure is formed by substitution but this may be classified into surface alloys; the c(2x2) structure can not be formed by simple substitution, because the clean Au(110) surface is reconstructed to form missing row of 1x2. In conclusion, the formation of surface alloys might occur generally for the AM adsorption on metal surfaces, depending on the combination of AM and substrate metal and temperature.

5. Summary

We have studied Li adsorption on Cu(001) at room temperature by using LEED and AES. LEED exhibits a sequential change with increasing Li coverage; 2x1, 3x3 and 4x4. In the 2x1 LEED pattern, weak streaky spots coexist. There observed two orthogonal domains for both the 2x1 and streaky structures. The 4x4 pattern disappears rather quickly with additional Li depositions, then the surface becomes disorder. On the other hand, at 180 K, the c(2x2) structure is formed first, then LEED pattern changes successively to structures denoted by matrices with increasing coverage. All these patterns at 180 K are originated from Li overlayers.

The 2x1 structure is the second observation for the system of alkali-metal adsorption on fcc(001) metal surfaces. The following features and behaviors of the streaky spots observed for Li/Cu(001) at 300 K are found to be very similar to those observed for systems of K or Cs adsorption on Ni(110) or Cu(110). (1) One basis vector of the unit mesh of the streaky spots coincides

with one basis vector of that for the 2x1 spots and does not shift as Li coverage increases. (2) The other basis vector points (2Θ 0.25) and shifts along the [1 0] direction within a limited coverage range of $0.375 \leq \Theta \leq 0.4$. (3) The streaky spots are elongated parallel to the [0 1] direction but are narrow across the [1 0] direction. (4) The streaky spots become distinct spots when the sample is cooled down to 180 K. (5) Even at 180 K the streaky spots shift with Li deposition on the 2x1 structure.

The strong similarity of the LEED features between two systems, *i. e.*, Li on Cu(001) and K or Cs on Ni(110) and Cu(110), leads to a suggestion for the structures of the 2x1 and streaky spots observed in this study; the 2x1 structure is due to a restructuring of missing-row type on the Cu(001) surface induced by Li adatoms and the streaky spots are originated from the Li atoms sitting in troughs formed by themselves.

The 3x3 and 4x4 structures are observed for the first time for the system of alkali-metal adsorption on fcc(001) metal surfaces. By examining the following conditions obtained from experimental facts, structure models for 3x3 and 4x4 are proposed; Li and Cu atoms are completely intermixed in the top layer on Cu(001) and they form ordered surface alloys with stoichiometry of LiCu. (1) The 3x3 and 4x4 structures are not due to Li overlayers but involve restructuring of the surface Cu atoms. (2) The 3x3 structure is formed naturally from the 2x1 structure. (3) The 4x4 structure is formed naturally from the 3x3 structure with increasing Li coverage. (4) The 3x3 and 4x4 structures are formed in limited ranges of Li coverage; $0.4 < \Theta(3x3) < \Theta(4x4) < 0.7$ where $\Theta(3x3)$ and $\Theta(4x4)$ mean Li coverages for the 3x3 and 4x4 structures, respectively. The formation of surface alloys might occur generally for the alkali-metal adsorption on metal surfaces, depending on the combination of alkali-metal and substrate metal and temperature.

References

[1] K. Müller, G. Besold and K. Heinz, in: Physics and Chemistry of Alkali Metal Adsorption, Eds. by H. P. Bonzel, A. M. Bradshaw and G. Ertl (Elsevier, Amsterdam, 1989) p. 65.

[2] For example: T. Aruga, H. Tochihara and Y. Murata, Surf. Sci. **158** (1985) 490.

[3] M. Okada, H. Tochihara and Y. Murata, Phys. Rev. **B43** (1991) 1411; Surf. Sci. 245 (1991) 380.

[4] R. Schuster, J. V. Barth, G. Ertl and R. J. Behm, Phys. Rev. **B44** (1991) 13689; Surf. Sci. 247 (1991) L229 and references therein.

[5] R. J. Behm, in Ref. [1] p. 111.

[6] C. J. Barnes, M. Lindroos, D. J. Holmes and D. A. King, in Ref. [1] p. 129.

[7] R. J. Behm, D. K. Flynn, K. D. Jamison, G. Ertl and P. A. Thiel, Phys. Rev. **B36** (1987) 9267.

[8] W. C. Fan and A. Ignatiev, Phys. Rev. **B38** (1988) 366.

[9] C. L. Fu and K. M. Ho, Phys. Rev. Lett. **63** (1989) 1617.

[10] K. W. Jacobsen and J. K. Nφrskov, Phys. Rev. Lett. **60** (1988) 2496.

[11] A. Schmalz, S. Aminpirooz, L. Becker, J. Haase, J. Neugebauer, M. Scheffler, D. R. Batchelor, D. L. Adams and E. Bφgh, Phys. Rev. Lett. **67** (1991) 2163.

[12] J. N. Andersen, M. Qvarford, R. Nyholm, J. F. van Acker and E. Lundgren, Phys. Rev. Lett. **68** (1992) 94.

[13] S. Mizuno, H. Tochihara, T. Kadowaki, H. Minagawa, K. Hayakawa, I. Toyoshima and C. Oshima, Surf. Sci. **264** (1992) 103.

[14] H. Tochihara and S. Mizuno, Chem Phys. Lett. **194** (1992) 51.

[15] S. Mizuno and H. Tochihara, to be published.

[16] H. Tochihara and Y. Murata, Surf. Sci. **215** (1989) L323.

[17] M. L. Shek, J. Hrbek, T. K. Sham and G. -Q. Xu, Surf. Sci., **234** (1990) 324.

[18] N. Fischer, S. Schuppler, R. Fischer, Th. Fautter and W. Steinmann, Phys. Rev. **B43** (1991) 14722.

[19] G. M. Watson, P. A. Bruhwiler, E. W. Plummer, H. -J. Sagner and K. -H. Frank, Phys. Rev. Lett., **65** (1990) 468.

[20] K. Y. Yu, W. E. Spicer, I. Lindau, P. Pianetta and S. F. Lin, Surf. Sci., **57** (1976) 157.

[21] S. Mizuno, H. Tochihara and T. Kawamura, Surf. Sci. **293** (1993) 239.

[22] T. B. Murray, L. H. Bonnett and H. Baker, Binary Alloy Phase Diagrams (American Society for Metals, 1986).

[23] P. Häberle and T. Gustafsson, Phys. Rev. **B40** (1989) 8218.

III. Approximate method for reducing the effect of beam-misalignment on low-energy electron diffraction *I(E)* curves at the normal incidence: the horizontal-beam method

An approximate method is proposed for measurement of intensity – energy (*I(E)*) curves of low-energy electron diffraction at normal incident condition. In this method only two equivalent spots located in the horizontal direction are optimized to have identical *I(E)* curves. It is found that *I(E)* curves obtained by this method approximate well those at the exactly normal incident condition, as far as the total misalignment is less than 1°. The reason for the success of this method is discussed. Advantages and disadvantages of this method are presented. It is emphasized that reproducible *I(E)* curves can be obtained easily because of a clear guideline of this method.

1. Introduction

Low-energy electron diffraction (LEED) has been the most powerful method for the determination of surface structures from the early stage of surface science. Up to 1992 more than 600 surface-structures have been determined, and in which more than a half has been studied by using LEED analysis [1]. The LEED analysis is carried out by comparing an experimental intensity – energy *I(E)* curve with theoretical curves obtained for various geometric models of a surface. The best-fit model is chosen as the structure of the surface. In this procedure of trial and error it is a problem that the best agreement between experimental and theoretical *I(E)* curves is not perfect. There are several probable reasons for the disagreement [2]. Since the theoretical curves are fitted to the experimental one, experimental errors should be reduced as much as possible. Especially, misalignment of an incident electron-beam to a sample is one of the most serious causes [3].

It is well known that a small tilt of a sample and a weak residual magnetic field does not ensure the normal incidence of the electron beam to the sample [3]. However, it is difficult to remove the tilt and magnetic field completely in an actual equipment or to estimate an angle of the shift from the normal. The difference from the normal incidence leads to a serious error in *I(E)* curves, because calculations are carried out at the exactly normal-incidence condition in order to reduce computing time. Previously, Davis and Noonan proposed an approximate method, in which intensities of equivalent spots are averaged [4], and we call it the averaging method here. Before averaging, the beam-alignment towards the normal should be optimized. They demonstrated that this method improves experimental *I(E)* curves well. However, the reason of the improvement is not clear, and it is tedious to repeat the alignment without a clear guideline. In the present paper we propose another approximate method for LEED *I(E)* measurement at a nearly normal-incidence condition. We call it the horizontal-beam method. The prominent feature of this method is clear-cutness of the procedure.

2. Experiment and Calculation

The Cu(001) surface was used as the substrate and cleaned with a standard procedure [5]. Sample cleanliness was confirmed with Auger electron spectroscopy and X-ray photoelectron spectroscopy, and no impurity was observed. LEED spots were very sharp with low background intensity.

LEED spot intensities were measured with a computer-controlled Auto-LEED system commercially available and based on the original design of the Erlangen group [6]. LEED *I(E)* curves were taken with an incident-energy range from 20 to 200 eV with 1 eV step. Sample temperature was 180 K during measurement.

Standard LEED programs [7] were used to calculate *I(E)* for the clean Cu(001) surface. Six phase shifts were used to calculate atomic scattering

(l_{max} = 5). The real part of the inner potential is determined during the course of the theory-experiment fit. The used Debye temperature of Cu is 335 K. The agreement between experimental and calculated $I(E)$ curves was tested by Pendry R-factor, R_P [8].

3. The Horizontal-Beam Method

A side-view of our experimental setup for the LEED $I(E)$ measurement is illustrated in Fig. 1(a). A rearview LEED optics (Omicron) is used, and LEED patterns are recorded with a CCD camera (Siemens) from rear side. The sample is set on a manipulator which has capability of translations along x, y and z directions and rotations on y axis (polar angle Θ) and on z axis (azimuthal angle Φ), as shown in Fig. 1(a). The manipulator does not provide a function of tilt. Usually LEED patterns like Fig. 1(b) are observed from fcc(001) surfaces. If the electron beam is incident exactly from the normal to the sample, $I(E)$ curves of four {1 0} spots shown in Fig. 1(b) would be identical. However, it is very difficult to achieve this because of the weak residual magnetic field and the tilt of the sample. In the averaging method one must try to adjust the manipulator in order to get four identical $I(E)$ curves of {1 0} spots as much as possible [4]. Since the guideline for achieving this is not clear, it is tedious to get convincing $I(E)$ curves of the four equivalent spots.

In the horizontal-beam method, the manipulator is rotated around z axis (azimuthal angle Φ) to line up (1 0) and ($\bar{1}$ 0) spots in the horizontal direction, as shown in Fig. 1(c). Then, the polar angle Θ is adjusted to get identical $I(E)$ curves of the two equivalent spots, (1 0) and ($\bar{1}$ 0). This procedure is quite easily carried out by using the auto-LEED system. Note that the tilt of the sample remains even after these procedures, as seen in Fig. 1(c). It is emphasized that $I(E)$ curves of (1 0) and ($\bar{1}$ 0) spots should be identical even under the presence of the tilt. In the condition of the horizontal-beam method,

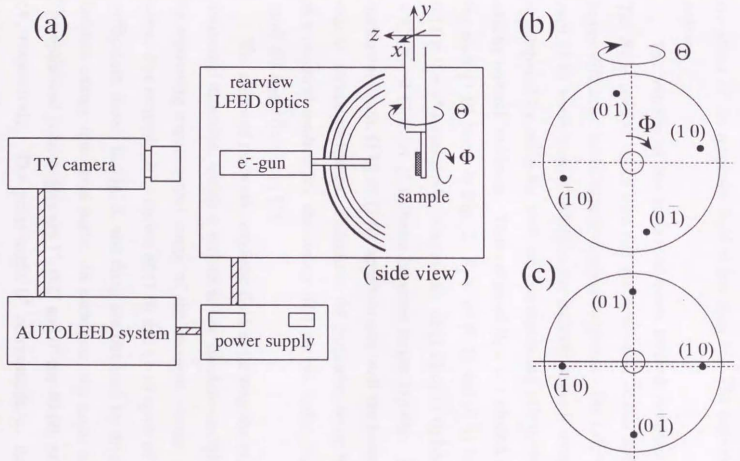

Fig. 1. (a) Side view of the experimental setup for LEED *I(E)* measurement and schematic diagram of the data acquisition system. Functions of the manipulator are indicated by x, y, z, Θ and Φ. (b) A typical arrangement of LEED spots from fcc(001). (c) An arrangement of LEED spots under the horizontal-beam condition. From the pattern, one can see that there is a tilt of the sample.

I(E) curves of (0 1) and (0 $\bar{1}$) spots are different each other and of course different from that of (1 0) or ($\bar{1}$ 0) spot. The existence of the residual magnetic field deflecting the electron beam in the vertical direction results in the same effect as the sample tilt. It should be confirmed that the tilt including the effect of the magnetic field is less than 1°. The reason for this is shown below.

The validity of the horizontal-beam method is demonstrated by Fig. 2. The R_P is used to make sure that the horizontal beams approximate well the beams diffracted at the exactly normal incidence. The calculated *I(E)* curve of each {1 0} beam from Cu(001) at the incident angle θ away from the normal is compared by using R_P with the corresponding calculated *I(E)* curve at the exactly normal incidence. Thus obtained R_P's are plotted as a function of θ for each {1 0} beam in Fig. 2. R_P's of (0 1) and (0 $\bar{1}$) beams are 0.14 and 0.11 at θ = 1° respectively, whereas R_P of (1 0) or ($\bar{1}$ 0) beam is 0.015. At θ > 1°, R_P of (1 0) or ($\bar{1}$ 0) beam becomes larger rapidly. It is clear that the horizontal beam, (1 0) or ($\bar{1}$ 0), approximates well the beams diffracted at the exactly normal incidence. Therefore, the horizontal-beam method can be used as a practical method for measuring *I(E)* curves under the existence of the small tilt angle (less than 1°).

The effect of the weak magnetic field deflecting the electron beam in the horizontal direction, which is serious at low incident-energies, can be reduced by separating experimental range of the incident energy into two or three parts. For example, *I(E)* curves of (1 0) and ($\bar{1}$ 0) spots of the clean Cu(001) surface are shown in Fig. 3, and these are obtained by dividing region of the incident energy into three parts. In each part, the polar angle is optimized. The optimized polar-angles are 1°, 0.2° and 0° for 40-60, 60-100 and 100-200 eV, respectively. The polar angle 0° corresponds to the horizontal-beam condition without the magnetic field deflecting the electron horizontally. It should be emphasized that the agreement of the two *I(E)* curves is excellent.

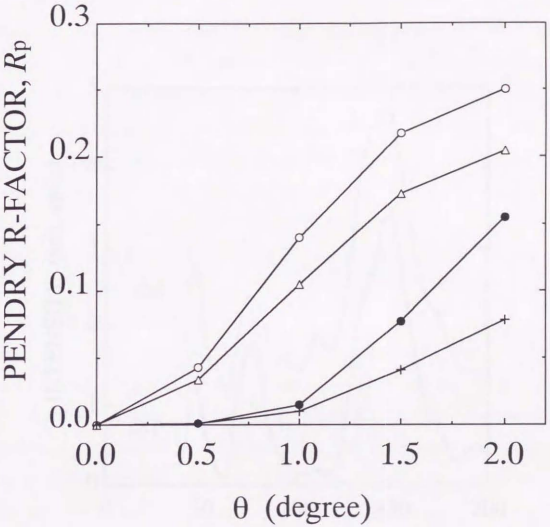

Fig. 2. Pendry R-factor, RP, as a function of q for examining the agreement of calculated *I(E)* curves of {1 0} beams from Cu(001) between at the exactly normal incidence and at the incident angle θ away from the normal under the horizontal-beam condition. (1 0) beam (solid circles), (0 1) beam (open circles) and (0 $\bar{1}$) beam (open triangles). The R-factor comparison is also made for the averaging method in a similar way (crosses); An average of calculated *I(E)* curve of four {1 0} beams at the same incident condition as that in the horizontal-beam method is compared with the calculated *I(E)* curve at the exactly normal incidence.

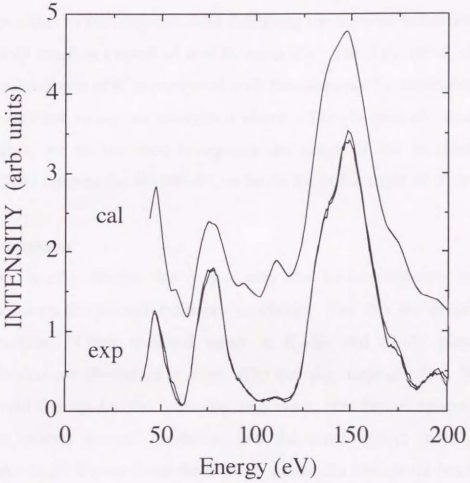

Fig. 3. Experimental *I(E)* curves (exp) of (1 0) and ($\bar{1}$ 0) beams from Cu(001) acquired under the horizontal-beam condition. Three *I(E)* curves obtained separately at the polar angle of 1°, 0.2° and 0° in energy ranges of 40-60, 60-100 and 100-200 eV, respectively, are combined for each (1 0) and ($\bar{1}$ 0) beam. The calculated *I(E)* curve (cal) of the {1 0} beam for the ideal structure of Cu(001) at the exactly normal incidence is also shown.

In addition, these are in good agreement with a calculated $I(E)$ curve at the exactly normal incidence for the bulk truncated structure of Cu(001), as shown in Fig. 3. The validity of using this structure as the clean Cu(001) surface becomes clear at section 5. In our equipment, however, it is found that the effect of the magnetic field deflecting the incident beam horizontally is negligibly small as a result of tests by using R_P. The $I(E)$ curve obtained at a fixed polar-angle of 0° is compared with that acquired by separating the range of the incident energy as mentioned above. The R_P between them is 0.005. Therefore, we do not need to separate the range of the incident energy to obtain $I(E)$ curves for 40-200 eV, as far as the polar angle of 0° is employed.

4. Discussion

We briefly discuss the reason why the horizontal-beam method well approximates the normal incidence condition. For this we make the Ewald construction. Cross sectional views in K_y-K_z and K_x-K_z planes for the construction are illustrated in Figs. 4(b) and (c), respectively. We consider the Ewald figures for the following two cases: one Ewald sphere (dotted) is for the exactly normal incidence, and the other sphere (solid) is for an incidence angle θ away from the normal under the horizontal-beam condition as illustrated in Fig. 4(a). The z axis in Fig. 4(a) is normal to the Cu(001) surface, and the plane (hatched) containing the z axis and the incident electron-beam is the yz plane. The corresponding reciprocal space is shown in Figs. 4(b) and (c). The reciprocal lattice rods of the {1 0} beams are depicted with solid vertical lines. The diffracted {1 0} beams are indicated in Figs. 4 (b) and (c) with dotted and solid arrows for the normal incidence and the incidence angle θ away from the normal, respectively. In each {1 0} beam the dotted and solid arrows touch different positions on the corresponding {1 0} rod, as seen in Figs. 4(b) and (c). The (1 0) and $(\bar{1}\ 0)$ beams correspond to the horizontal beams.

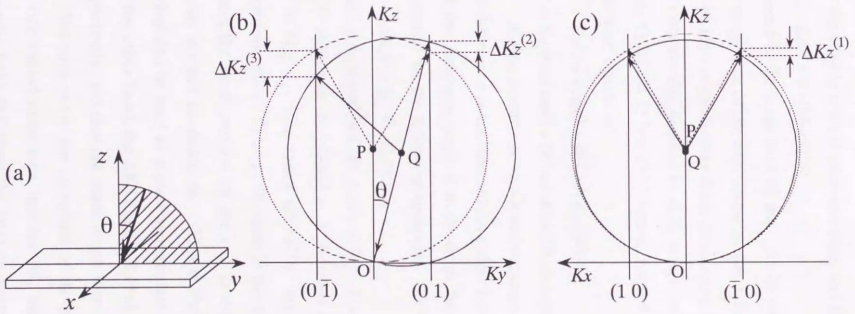

Fig. 4. (a) The geometry of the beam incidence in the horizontal-beam condition. The incident beam is in the *yz* plane (hatched) and with an angle θ away from the sample normal. (b) Cross sectional representation of the Ewald construction for the horizontal-beam method together with that for the exactly normal incidence in *Ky-Kz* plane. Points P and Q are centers of the Ewald spheres for the normal incidence and the horizontal-beam conditions, respectively. See text in detail. (c) same as (b) but in *Kx-Kz* plane. Note that point Q and solid arrows are not in the*Kx-Kz* plane.

The positions of the intersection on the diffraction rods are denoted as $K_z^{(0)}$ for the exactly normal incidence case, and this is given by:

$$K_z^{(0)} = k+(k^2-n^2)^{1/2}, \quad (1)$$

where k is the magnitude of the wave-vector of the incident electron and n is the magnitude of the unit vector of the 2-dimensional reciprocal lattice. For the incident angle θ away from the normal, the positions of the intersection on the rods are also denoted as $K_z^{(i)}$, where i =1, 2, and 3 corresponds to the (1 0) or ($\bar{1}$ 0), (0 1) and (0 $\bar{1}$) beams, respectively. These are expressed by the following equations:

$$K_z^{(1)} = k\cos\theta + (k^2-n^2-k^2\sin^2\theta)^{1/2}, \quad (2)$$

$$K_z^{(2)} = k\cos\theta + (k^2-n^2-k^2\sin^2\theta+2nk\sin\theta)^{1/2}, \quad (3)$$

$$K_z^{(3)} = k\cos\theta + (k^2-n^2-k^2\sin^2\theta-2nk\sin\theta)^{1/2}. \quad (4)$$

The difference in the intersection points between the exactly normal incidence and the incidence angle θ away from the normal for each {1 0} beam is expressed by the following equation:

$$\Delta K_z^{(i)} = |K_z^{(0)}- K_z^{(i)}|. \quad (5)$$

$\Delta K_z^{(i)}$ is indicated in Figs. 4(b) and (c). The $\Delta K_z^{(2)}$ and $\Delta K_z^{(3)}$ are larger than $\Delta K_z^{(1)}$ and these are plotted as a function of θ at the incident energy of 100 eV in Fig. 5. The values of $\Delta K_z^{(1)}$ are less than 0.002 Å^{-1} below 1°. Therefore, the (1 0) or ($\bar{1}$ 0) beam at the horizontal-beam condition explores almost the same position on the rod profile as the beams diffracted at the exactly normal incidence do. This is the reason why the horizontal beam method can be used as a good approximate method for the normal incidence. On the other hand, the $\Delta K_z^{(2)}$ and $\Delta K_z^{(3)}$ at θ = 1° are 0.047 and 0.051 Å^{-1}, respectively, and they are much larger than that of the $\Delta K_z^{(1)}$.

We summarize the procedure of the horizontal-beam method. First of all, one should make sure that the tilt, including the effect of the residual magnetic field deflecting the electron beam in the vertical direction, is less than 1°, otherwise the horizontal-beam method is not a good approximate

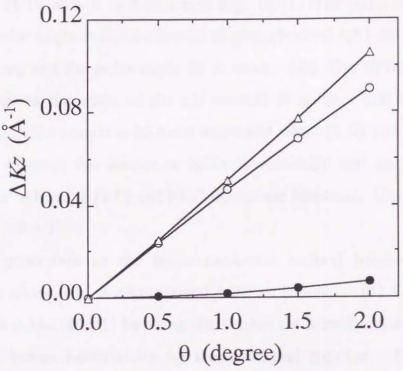

Fig. 5 $\Delta K_z^{(i)}$ versus θ for (1 0) or ($\bar{1}$ 0) beams (i=1, solid circles), (0 1) beam (i=2, open circles) and (0 $\bar{1}$) beam (i=3, triangles) at the incident energy of 100 eV. The definitions of $\Delta K_z^{(i)}$ where i=1, 2, 3 are shown in text and also in Figs. 4(b) and (c).

method for the normal incidence. The reason for this is already argued at section III with Fig. 2. To find the angle of the tilt, the following procedures can be carried out. (i) The polar angle (Θ) is adjusted to give identical $I(E)$ curves of (1 0) and (0 1) beams (see Fig. 1(c)). The polar angle Θ_0 is read. (ii) The polar angle is again adjusted to give identical $I(E)$ curves of (1 0) and ($\bar{1}$ 0) beams, and the polar angle Θ_1 is read. (iii) The difference ($\Theta_1 - \Theta_0$) corresponds to the angle of the tilt wanted. It is clear that the procedure is appropriate; the sample is inclined vertically when (1 0) and ($\bar{1}$ 0) beams are identical, whereas the sample is inclined vertically and horizontally by the same angle when the (1 0) and (0 1) beams are identical. Usually we obtained the tilt of 0.5 ~ 1°.

The procedure of the horizontal-beam method becomes clear in the discussion above and is summarized here as follows. (1) Confirm that the overall tilt is less than 1° by using the procedure mentioned above. (2) Align the target beams horizontally by the azimuthal rotation. (3) Optimize the polar angle to give identical $I(E)$ curves of two equivalent beams. (4) Average thus obtained two $I(E)$ curves. (5) Repeat the procedure (4) for beams in the same azimuthal direction. (6) Repeat the procedure (2) to (5) for beams in other azimuthal directions.

It is interesting to compare the horizontal-beam method with the averaging method. The reliability of the averaging method can be also examined by using R_P. That is, the calculated $I(E)$ curve, which is obtained by averaging four {1 0} beams from Cu(001) at the incident angle θ away from the normal, is compared with that at the exactly normal incidence. The results are shown also in Fig. 2 with crosses. Thus obtained values are almost the same as those obtained with the horizontal-beam method at $\theta < 1°$. This indicates that the horizontal-beam method is a good approximate method as the averaging method.

We should point out advantages and disadvantages of the horizontal-beam method in comparison with the averaging method. The advantages are the following: (1) The guideline for achieving the condition is clear and simple, which ensures the reproducibility of $I(E)$ curves. (2) It is easy to judge that the two $I(E)$ curves of the equivalent beams are identical. (3) The reason why the horizontal-beam method is a good approximate method is clear. On the other hand, the disadvantages are as follows: (1) The capability of the azimuthal rotation is necessary for the manipulator. (2) Adjustment of the azimuthal angle should be repeated for beams belonging to different azimuthal directions. (3) The horizontal-beam method can not be used for surfaces having a three-fold symmetry.

5. Application

5.1. Structure determination of the clean Cu(001) surface

The horizontal-beam method is first applied for structure-determination of the clean Cu(001) surface. Agreement between theory and experiment was tested by R_P analysis [8] of two integral-order beams {1 0} and {1 1}. The averaged R_P is calculated as a function of the interlayer spacing between the first and second Cu layer, d_{12}, with 0.05 Å step. Thus obtained d_{12} is 1.80 Å. The interlayer spacing between the second and third layers is also determined under the condition of d_{12} = 1.80 Å. The minimum R_P is obtained at d_{23} = 1.80 Å. These spacings are almost the same as the bulk value, 1.807 Å and are in good agreement with the previous studies [9,10]. This is the reason why we can use the bulk truncated structure as the real structure of Cu(001) to check for the validity of the horizontal-beam method, as mentioned in section 3. The minimum R_P is 0.113 at $d_{12} = d_{23}$ = 1.80 Å. Another R-factor of Zanazzi and Jona [11] is 0.037 and this value is similar to that in the literature, 0.049 [9,10]. Therefore, it is clear that the horizontal-beam method can be

used as a good approximate method for the nearly normal-incident LEED $I(E)$ measurement.

It is interesting to estimate the contribution of the horizontal method into the value of the best-fit R_P (0.113 for the Cu(001) surface). In the present study, we confirm that the tilt from the normal is 1°, and this makes worse the agreement of the experimental $I(E)$ curves under the horizontal-beam condition with those at the exactly normal incidence by an amount of 0.015 in R_P, as seen in Fig. 2. In addition, the use of the fixed polar-angle of 0° for an incident energy range of 40 – 200 eV introduces another disagreement by an amount of 0.005 into R_P, as mentioned in section 3. Total error introduced by using the horizontal-beam method corresponds to the amount of 0.020 in R_P, and this is less than 20% of the best-fit R_P for the clean Cu(001) surface. Therefore, it is concluded that the horizontal-beam method dose not introduce significant errors. Major errors comes from another sources in experiment and calculation.

5.2. Other examples for surface structure determination

Furthermore, the horizontal-beam method has been successfully used to determine surface structures of the c(2x2) and (2x1) structures formed by Li deposition on Cu(001) at 180 and 300 K, respectively [12-14]. Their details will be described in Chapters IV and V.

6. Summary

We have proposed a very practical method for the accurate measurement of LEED intensity – energy ($I(E)$) curves at nearly normal incidence under the existence of the weak residual magnetic field and tilt of the sample. In this method only two equivalent beams located in the horizontal direction are optimized to have identical $I(E)$ curves. It is found that $I(E)$ curves acquired by this method approximates well those at the exactly normal incident

condition, as far as the total misalignment is less than 1°. The reason for the success of this method is that the beams in the horizontal direction explore almost the same position of the rod profile as those at the exactly normal incidence do. It is estimated that the error introduced by the horizontal-beam method into the experimental *I(E)* curve amounts to only less than 20% of the best-fit value (0.113) of the Pendry *R*-factor, for the case of the clean Cu(001) surface. It is emphasized that reproducible *I(E)* curves can be obtained easily because of the clear guideline of this method.

References

[1] M. A. Van Hove, private communication.

[2] P. M. Marcus and F. Jona, *Determination of surface structure by LEED*, (Plenum Press, New York, 1984).

[3] K. Heinz and K. Müller, *Structural studies of surfaces*, (Springer, Berlin, 1982), p. 1.

[4] H. L. Davis and J. R. Noonan, Surf. Sci. **115** (1982) L75.

[5] H. Tochihara and S. Mizuno, Surf. Sci. **279** (1992) 89.

[6] K. Müller and K. Heinz, Springer Series in Surface Sciences, Vol. **2** (Springer, Berlin, 1985) p. 105.

[7] M. A. Van Hove and S. Y. Tong, Springer Series in Chemical Physics, Vol. **2**, *Surface Crystallography by LEED,* (Springer, Berlin, 1979).

[8] J. B. Pendry, J. Phys. **C 13** (1980) 937.

[9] F. Jona, Surf. Sci. **192** (1987) 398.

[10] F. Jona, P. Jiang and P. M. Marcus, Surf. Sci. **192** (1987) 414.

[11] E. Zanazzi and F. Jona, Surf. Sci. **62** (1977) 61.

[12] H. Tochihara and S. Mizuno, Surf. Sci. **287/288** (1993) 423.

[13] S. Mizuno, H. Tochihara and T. Kawamura, Surf. Sci. **293** (1993) 239.

[14] S. Mizuno, H. Tochihara and T. Kawamura, Surf. Sci. **292** (1993) L811.

IV. Determination of the c(2x2) structure formed on Cu(001) upon Li adsorption: a low-energy electron diffraction analysis

We have determined the c(2x2) structure formed on Cu(001) upon Li adsorption at 180 K by low-energy electron diffraction analysis. It is found that an overlayer of Li atoms sitting on the fourfold hollow sites (coverage 0.5) is preferred with the Cu-Li interlayer spacing of 1.96 ± 0.08 Å. The radius of the Li atom is 92% of the Li metallic one. The interlayer spacing between the first and second layers of Cu(001) is 1.81 ± 0.04 Å, and this is the same value of the spacing of the clean Cu(001) surface.

1. Introduction

It is an outstanding feature of alkali-metal (AM) atom adsorption on metal surfaces that various ordered structures appear with increasing AM coverage [1]. Even at low coverages where low-energy electron diffraction (LEED) patterns do not exhibit spots, halos change their diameters as a function of coverage [2,3]. The successive change of the surface structure implies that AM adatoms are distributed uniformly on the surfaces and that the mean distance between AM adatoms decreases gradually.

So far as mentioned above AM adatoms on metal surfaces have been considered to form overlayers, in which AM adatoms are located preferentially on the highest coordination site except for the high coverage regime. However, recent surface-structure determination techniques such as LEED analysis [4-10], surface extended X-ray absorption fine structure (SEXAFS) measurement [11-13] and normal-incidence standing X-ray wavefield absorption (NISXW) [14,15] have clarified that the top-site adsorption [4,8-10,14] and substitutional adsorption [5-7,10,12,15] take place as well as the overlayer formation for several adsorption systems. Therefore, the check with structure determination techniques is required even for

structures whose periodicities are familiar in the AM adsorption systems. It should be noted also that there has been rather small number of structural determinations of the ordered structures formed upon AM adsorption [4-19].

As described in Chapter II, we have studied the adsorption of Li on Cu(001) at 180 and 300 K mainly with LEED observations [20-22]. It was found that LEED exhibits completely different patterns from the Li covered surfaces at two temperatures; At 180 K the first superstructure is c(2x2), then the LEED pattern changes successively to structures denoted by matrices with increasing coverage [23]. At 300 K LEED exhibits superstructures of 2x1, 3x3 and 4x4. We will describe the determination of the (2x1) structure with LEED analysis in Chapter IV [21,22]. It is concluded that the (2x1) structure is ascribed to the missing-row type restructuring of the top layer of Cu(001) induced by Li adsorption and that Li atoms are located in troughs formed by themselves. That is, Li adatoms do not form overlayers but substitute Cu atoms in the top layer at room temperature. The (3x3) and (4x4) structures formed at higher Li coverages have been assigned to ordered surface-alloys [20].

In a previous preliminary study we have proposed that the c(2x2) structure formed at 180 K is due to Li adatoms sitting on fourfold hollow sites by LEED analysis [21]. However, we did not optimize the geometry and did not examine the interlayer spacings of Cu(001). It is required to determine the detailed structure of the c(2x2) structure formed at low temperature. In addition, we have found that the c(2x2) structure converts to the (2x1) structure irreversibly at about 200 K upon annealing [20]. The (2x1) structure is the same one whose structure is the missing-row type restructuring as mentioned above. Therefore, it is interesting to find some possible indications of the restructuring of the substrate surface in the c(2x2) structure as well as to determine the convincing adsorption-site of Li by LEED analysis.

2. Experiment and Calculation

The experiments were carried out in a three-level UHV chamber equipped with LEED, Auger electron spectroscopy (AES), angle-resolved photoelectron spectroscopy, X-ray photoelectron spectroscopy (XPS) and high-resolution electron energy-loss spectroscopy [24]. The Cu(001) surface was cleaned with a standard procedure [20,24]. Sample cleanliness was confirmed with AES and XPS and no impurity was observed. LEED spots were very sharp with low background intensity. Li was deposited onto the surface from a commercial SAES dispenser at 180 K. During Li deposition the pressure was less than 1.5×10^{-10} Torr. Since water in the chamber is the most active species for the Li covered Cu surface [24,25], a liquid-nitrogen shroud was used to remove the water. Then, a partial pressure of water was less than 3×10^{-12} Torr.

LEED spot intensities were measured with a computer-controlled Auto-LEED system commercially available and based on the original design of the Erlangen group [26]. LEED intensity-energy curves, *I(E)*, were taken at the normal incidence with incident-energy range from 20 to 200 eV and with 1 eV step. Sample temperature was 180 K during measurement. Normal-incidence condition was achieved approximately by using the horizontal-beam method, in which only two equivalent spots located in the horizontal direction are measured and averaged. Details of the horizontal-beam method has been described in Chapter III.

Standard LEED programs [27] were used to calculate *I(E)* for the clean Cu(001) surface and the c(2x2) structure formed upon Li adsorption. Six phase shifts were used to calculate atomic scattering ($l_{max} = 5$). The real part of the inner potential is determined during the course of the theory-experiment fit. The Debye temperature of Cu is 335 K. The Debye temperature of the Li overlayer is optimized to 480 K as described later.

3. Structure of the c(2x2)Li/Cu(001) Surface

LEED intensity calculations were performed for Li overlayers at the fourfold hollow and atop sites for the c(2x2) structure. At first we used the bulk Li Debye temperature, 316 K, for the Li overlayer. Agreement between theory and experiment was examined also by R_P analysis that included two integral-order beams of {1 0} and {1 1} and one half-order beam of {0.5 0.5}. The precision of the structure parameters was determined by a sensitive analysis which is based on the steepness of the R_P minimum [28]. The R_P minima are compared for the Li overlayers at the hollow and atop sites as a function of the interlayer spacing between the Li adlayer and the first Cu layer, $d_{Li\text{-}Cu}$. For these sites the adsorbate height was varied in steps of 0.1 Å, and it is found that a deeper minimum was obtained for the hollow site. By using the geometry thus obtained we calculated R_P as a function of the Debye temperature of the Li overlayer as shown in fig. 1. The Debye temperature of the Li monolayer was determined to be 480 K. The Li Debye temperature of the overlayer is higher than the bulk value, and this increase is similarly observed in the K overlayer on Ni(001) [18] where the K Debye temperature optimized is 200 K while 91 K of the K bulk metal. Then, we calculated again the *I(E)* curves of the c(2x2) structure at the hollow and atop sites with the Li Debye temperature of 480 K. At this time for these sites the adsorbate height was varied in steps of 0.02 Å over a range that was chosen from reasonable Li-Cu bond lengths according to a hard-sphere model of the atoms. Minima of R_P' s are 0.106 and 0.26 for the hollow and atop sites, respectively, as shown in fig. 2. The R_P for the hollow site has a steep minimum at $d_{Li\text{-}Cu}$ = 1.96 Å, whereas the R_P for the atop site indicates a shallow minimum at $d_{Li\text{-}Cu}$ = 2.7 Å. Furthermore, it should be noted that each beam for the atop site has a different minimum position. These facts mentioned above clearly indicate

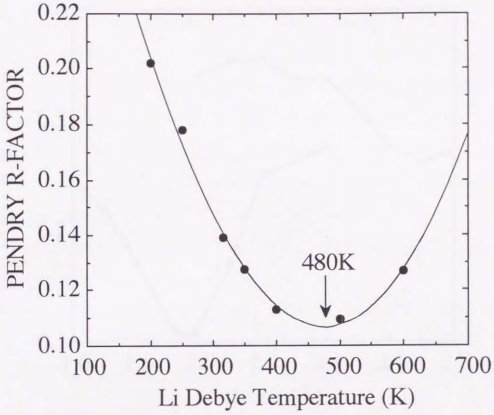

Fig. 1. Pendry R-factor, R_P, as a function of the Debye temperature of the Li overlayer. R_P is the average of R_P's of {1 0}, {1 1} and {0.5 0.5} spots of the c(2x2) structure formed upon Li adsorption on Cu(001).

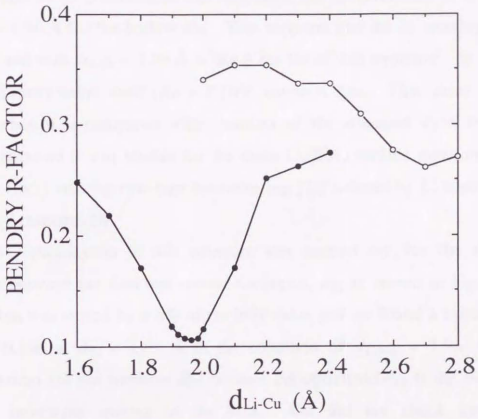

Fig. 2. The variations of the Pendry R-factor, R_P, with the interlayer spacing between the Li adlayer and the first Cu(001) layer, $d_{Li\text{-}Cu}$, for the overlayer structures at the hollow (solid circles) and atop (open circles) sites. R_P is the average of R_P's of {1 0}, {1 1} and {0.5 0.5} spots of the c(2x2) structure formed upon Li adsorption on Cu(001).

that the Li overlayer at the atop site is not likely as the c(2x2) structure.

The R_P shown in Fig. 2 is the average of the three beams mentioned above, and we have confirmed that each beam has the minimum of R-factor at $d_{Li\text{-}Cu}$ = 1.96 Å for the hollow site. This supports that the Li overlayer at the hollow site with $d_{Li\text{-}Cu}$ = 1.96 Å is likely for the c(2x2) structure. In addition, the minimum value itself (R_P = 0.106) supports this. This value is pretty good, when it is compared with minima of the averaged R_P's, 0.113 and 0.168, obtained in our studies for the clean Cu(001) surface mentioned above and the (2x1) missing-row-type restructuring [22] induced by Li adsorption on Cu(001), respectively.

The optimization of this structure was carried out for the interlayer spacing between the first and second Cu layers, d_{12} as shown in fig. 3. The relaxation was varied by ± 6% of the bulk value and we found a minimum of R_P = 0.106 at d_{12} = 1.81 Å in the condition of $d_{Li\text{-}Cu}$ = 1.96 Å. This optimization did not improve R_P, because the optimized d_{12} is the same value of the interlayer spacing of the bulk. We did not check any lateral displacement because of limitation of the present calculation. The optimum structural parameters for the c(2x2) structure together with the errors are the following; $d_{Li\text{-}Cu}$ = 1.96 Å ± 0.08 Å and d_{12} = 1.81 ± 0.04 Å. The errors were estimated from the total energy range ΔE = 460 eV using the variance of R_P-factor $\Delta R = R(8V_{oi}/\Delta E)^{1/2}$, where R is the minimum R_P-factor achieved [28] and the imaginary part of the inner potential V_{oi} was chosen to be proportional to $E^{1/3}$. Because of the rather small value of ΔE the error limits are rather high (ΔR = 0.03). A comparison of the experimental $I(E)$ curves with those calculated for the optimum geometry is shown in fig. 4, from which a very good agreement is evident.

4. Discussion

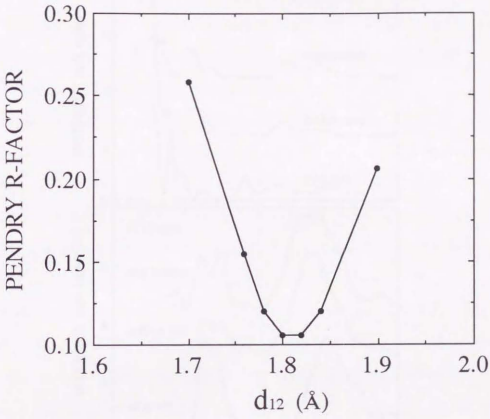

Fig. 3. The variation of the Pendry R-factor with the first interlayer spacing of Cu(001), d_{12}, for the overlayer structures at the hollow sites at $d_{Li\text{-}Cu_1} = 1.96$ Å. R_P is the average of R_P's of {1 0}, {1 1} and {0.5 0.5} spots of the c(2x2) structure formed upon Li adsorption on Cu(001).

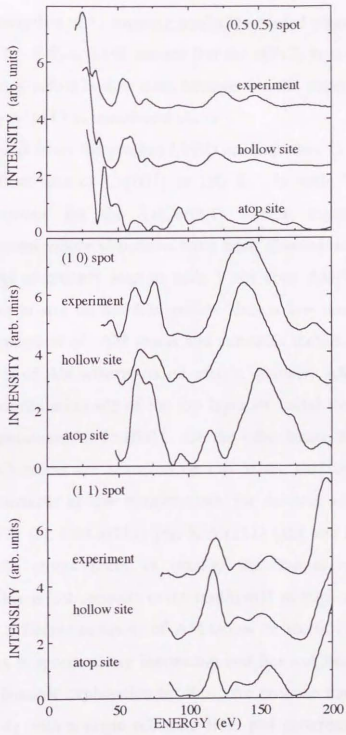

Fig. 4. *I(E)* curves as measured and calculated for the best fit for hollow and atop sites (adsorption at the hollow sites with $d_{Li\text{-}Cu} = 1.96$ Å and $d_{12} = 1.81$ Å).

For the c(2x2) structure we did not check for restructuring models of the Cu(001) surface induced by Li adsorption; A possible model would be substitutional adsorption of Li forming a c(2x2) ordered phase. However, the level of the best fit of $R_P = 0.106$ assures that the c(2x2) structure is due to Li adsorption on the fourfold hollow sites, because for the clean Cu(001) surface the minimum R_P is 0.113 as mentioned above.

It is concluded from the present LEED analysis that Li adatoms occupy the fourfold hollow sites of Cu(001) at 180 K. In table 1 we summarize structural parameters for the Li/Cu(001) system together with other AM/fcc(001) systems whose structures have been determined at low sample-temperatures. As commonly seen in table 1 for four AM/fcc(001) systems, AM atoms prefer to stay on fourfold hollow sites at low temperatures. This seems to be independent of AM atoms and substrate metals. Therefore, the traditional picture of AM adsorption on metals, namely, AM adatoms reside on the highest coordination site of the top layer of metal surfaces, is true at low sample-temperatures for fcc(001). On the other hand, it should be noted that K, Rb and Cs atoms are adsorbed on top of the surface metal atoms of fcc(111) metal surfaces at low temperatures for several adsorption systems such as K/Ni(111) [8], Cs/Cu(111) [4], K/Al(111) [10] and Rb/Al(111) [14]. On fcc(111) AM atoms seem to occupy the lowest coordination site preferentially. This is just opposite to the traditional picture mentioned above. This completely different behavior of AM atoms on fcc(001) and fcc(111) at low temperatures is spectacularly interesting and has not been explained yet. Here, we give a possible explanation for this. We propose that an AM adatom is bonded not only with a single substrate-atom just underneath but also with surrounding six substrate-atoms as shown in fig. 5 with hatched circles. The existence of a rumpling of the top layer of fcc(111) shown in fig. 5(b) has been confirmed by LEED analysis [10]. The rumpling shown in fig. 5 is exaggerated in order to indicate the bonds between the AM adatom and the six

Table 1

Structure determinations for alkali-metal (AM) adsorption on fcc(001) metals at low temperatures.

System	Structure	Site	Coverage	AM radius[a]	r/r_0 [b]	Δd_{12}[c]	Δd_{12} (clean)	Temperature	Method	Ref.
Li/Cu(001)	c(2x2)	Hollow	0.5	1.39±0.08Å	92%	(0±2)%	0%	180 K	LEED	This work
Na/Al(001)	c(2x2)	Hollow	0.5	1.78±0.03Å	97%	—	0%[d]	140 K	SEXAFS	[13]
K/Ni(001)	c(4x2)	Hollow	0.25	1.96±0.05Å	87%	(0±2)%	0%[d]	90 - 200K	LEED	[18]
Cs/Rh(001)	c(4x2)	Hollow	0.25	2.10±0.06Å	80%	(-0.5±2)%	(0.5±2)%	120K	LEED	[16]

[a] The radius of AM adatom is obtained by subtracting the metallic radius of the substrate atom [34] from the bond length determined between the AM and substrate atoms.

[b] Ratio of AM adatom radius (r) to bulk AM radius (r_0). r_0's are 1.51, 1.83, 2.26 and 2.62 Å for Li, Na, K and Cs bulk metals, respectively [34].

[c] Relaxation of the first interlayer spacings of substrates with AM overlayers.

[d] Ref. 35.

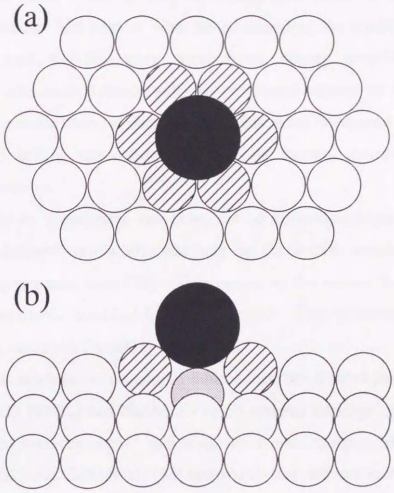

Fig. 5. Illustrations for explaining why an alkali-metal (AM) adatom is stabilized on top of a single substrate-atom in fcc(111) surfaces. (a) Top view. Solid and open circles are AM and substrate atoms, respectively. Six hatched-circles are substrate atoms interacting with the AM adatom. Diameters of the AM and substrate atoms are chosen to be those of K and Al. (b) Cross sectional view along line XY indicated in (a). A dotted circle is the substrate atom just underneath the AM adatom. The rumpling in the top layer of the substrate is indicated.

substrate-atoms clearly. Anyway it is the point that there is the rumpling in the top layer of the substrate surfaces underneath AM overlayers at low temperatures. This rumpling may be created as a result of some bonding-interactions of the AM adatom with the surrounding six substrate-atoms. If this idea is true, the AM atom occupies the highest coordination site on fcc(111) surfaces in accordance with the traditional picture of AM adsorption above. The coordination number in this case is seven compared with three for the threefold hollow site considered to be the highest coordination site on fcc(111) otherwise.

It should be mentioned, however, that at coverages higher than 0.5 Li adatoms are located on Cu(001) not only on the hollow site but also on the bridge or asymmetric sites [23]. This is due to the reason that there is no hollow-site available for Li at higher coverages. This phenomenon has been observed for other AM/fcc(001) systems [1].

The four adsorption systems in table 1 can be divided into two groups: the Li/Cu(001) [20-22] and Na/Al(001) [13] systems undergo restructuring of the substrate surfaces upon annealing to room temperature, while the K/Ni(001) [32] and Cs/Rh(001) [33] systems do not convert to new structures. It is interesting to compare the structural parameters between the two systems. The ratio (r/r_0) of the radius (r) of the AM adatom determined to that (r_0) of the bulk AM is listed in table 1. There is a tendency that AM atoms in the Li/Cu(001) and Na/Al(001) systems have closer radii to metallic ones than the other group does, but it is dangerous to conclude this because of small number of examples. The changes (Δd_{12}) of the first interlayer spacing of the substrate surfaces after AM adsorption from the bulk values are also listed in table 1 together with Δd_{12} of the clean substrate surfaces. In both groups the first interlayer spacings do not change after AM adsorption and are almost the same as the bulk values. Therefore, there seems to be no clear difference in structure parameters between the two adsorption systems.

Finally, we would like to note again that in the present Li/Cu(001) system it has been confirmed that the c(2x2) structure converts to the (2x1) structure at about 200 K [20]. The fact that the first interlayer spacing obtained at 180 K is not expanded underneath the Li monolayer even on the verge of the restructuring suggests the following idea: the restructuring does not take place uniformly. That is, the unstabilization of the top layer of Cu(001) due to Li adsorption may not be the driving force for this restructuring.

5. Conclusion

We have determined the c(2x2) structure formed on Cu(001) upon Li adsorption at 180 K by LEED analysis. It has been known that at about 200 K the c(2x2) structure changes to the (2x1) structure irreversibly caused by the missing-row type restructuring of the top layer of Cu(001). It is found for the c(2x2) structure that an overlayer of Li atoms sitting on the fourfold hollow sites (coverage 0.5) is preferred with the Cu-Li interlayer spacing of 1.96 Å. The radius of the Li atom is 92% of a Li metallic one. The first interlayer spacing of Cu(001) is not affected by the Li overlayer and any indication of the restructuring is not found in the c(2x2) structure.

It is concluded that for AM/fcc(001) systems AM atoms prefer to reside on the highest coordination site at low temperatures. This conclusion is consistent with the traditional picture of AM adsorption on metal surfaces. We comment that this picture may be also realized for the on-top site adsorption of AM atoms on fcc(111) metal surfaces reported for several systems.

References

[1] K. Müller, G. Besold and K. Heinz, in: Physics and Chemistry of Alkali Metal Adsorption, Eds. by H. P. Bonzel, A. M. Bradshaw and G. Ertl (Elsevier, Amsterdam, 1989) p. 65.

[2] For example: R. L. Gerlach and T. N. Rhodin, Surf. Sci. **17** (1969) 32.

[3] Exceptionally, for K/Cu(001) it was found that the diameter of the halo does not change at room temperature. See: T. Aruga, H. Tochihara and Y. Murata, Surf. Sci. **175** (1986) L725.

[4] S. Å. Lindgren, L. Wallden, J. Rundgren, P. Westrin and J. Neve, Phys. Rev. **B28** (1983) 6707.

[5] C. J. Barnes, M. Lindroos and D. A. King, Surf. Sci. **201**(1988) 108.

[6] C. J. Barnes, M. Lindroos, D. J. Holmes and D. A. King, Surf. Sci. **219** (1989) 143.

[7] Z. P. Hu, B. C. Pan, W. C. Fan and A. Ignatiev, Phys. Rev. **B41** (1990) 9692.

[8] H. Over, H. Bludau, M. Skottke-Klein, G. Ertl, W. Moritz and C. T. Campbell, Phys. Rev. **B45** (1992) 8638.

[9] D. Fisher, S. Chandavarkar, I. R. Collins, R. D. Diehl, P. Kaukasoina and M. Lindroos, Phys. Rev. Lett. **68** (1992) 2786.

[10] C. Stampfl, M. Scheffler, H. Over, J. Burchhardt, M. Nielsen, D. L. Adams and W. Moritz, Phys. Rev. Lett. **69** (1992) 1532.

[11] A. Schmalz, S. Aminpirooz, L. Becker, J. Haase, J. Neugebauer, M. Scheffler, D. R. Batchelor, D. L. Adams and E. Bϕgh, Phys. Rev. Lett. **67** (1991) 2163.

[12] A. Schmalz, S. Aminpirooz, L. Becker, J. Haase, D. R. Batchelor, D. L. Adams and E. Bϕgh, Surf. Sci. **269/270** (1992) 659.

[13] S. Aminpirooz, A. Schmalz, L. Becker, N. Pangher, J. Haase, M. M. Nielsen, D. R. Batchelor, E. Bϕgh and D. L. Adams, Phys. Rev. **B46** (1992) 15594.

[14] M. Kerkar, D. Fisher, D. P. Woodruff, R. G. Jones, R. D. Diehl and B. Cowie, Phys. Rev. Lett. **68** (1992) 3204.

[15] M. Kerkar, D. Fisher, D. P. Woodruff, R. G. Jones, R. D. Diehl and B. Cowie, Surf. Sci. **278** (1992) 246.

[16] C. von Eggeling, G. Schmidt, G. Besold, L. Hammer, K. Heinz and K. Müller, Surf. Sci. **221** (1989) 11.

[17] C. J. Barnes, P. Hu, M. Lindroos and D. A. King, Surf. Sci. **251/252** (1991) 561.

[18] U. Muschiol, P. Bayer, K. Heinz, W. Oed and J. B. Pendry, Surf. Sci. **275** (1992) 185.

[19] M. Gierer, H. Bludau, H. Hertel, H. Over, W. Moritz and G. Ertl, Surf. Sci Lett. **279** (1992) L170.

[20] H. Tochihara and S. Mizuno, Surf. Sci. **279** (1992) 89.

[21] H. Tochihara and S. Mizuno, Surf. Sci. **287/288** (1993) 423.

[22] S. Mizuno, H. Tochihara and T. Kawamura, Surf. Sci. **293** (1993) L811.

[23] S. Mizuno and H. Tochihara, to be published.

[24] S. Mizuno, H. Tochihara, T. Kadowaki, H. Minagawa, K. Hayakawa, I. Toyoshima and C. Oshima, Surf. Sci. **264** (1992) 103.

[25] H. Tochihara and S. Mizuno, Chem. Phys. Lett. **194** (1992) 51.

[26] K. Müller and K. Heinz, Springer Series in Surface Sciences, Vol. **2** (Springer, Berlin, 1985) p. 105.

[27] M. A. Van Hove and S. Y. Tong, Springer Series in Chemical Physics, Vol. **2**, Surface Crystallography by LEED (Springer, Berlin, 1979).

[28] J. B. Pendry, J. Phys. **C 13** (1980) 937.

[29] F. Jona, Surf. Sci. **192** (1987) 398.

[30] F. Jona, P. Jiang and P. M. Marcus, Surf. Sci. **192** (1987) 414.

[31] E. Zanazzi and F. Jona, Surf. Sci. **62** (1977) 61.

[32] D. Fisher and R. D. Diehl, Phys. Rev. **B46** (1992) 2512.

[33] G. Besold, Th. Schaffroth, K. Heinz, G. Schmidt and K. Müller, Surf. Sci. **189/190** (1987) 252.

[34] C. Kittel in: Introduction to Solid State Physics, 6th ed. (Wiley, New York, 1986).

[35] M. A. Van Hove, W. H. Weinberg and C. - M. Chan, Low-Energy Electron Diffraction, (Springer, Berlin Heiderberg, 1986) p. 256.

V. Missing-row-type restructuring of the Cu(001) surface induced by Li adsorption: a low-energy electron diffraction analysis

The 2x1 structure formed on a Cu(001) surface upon Li deposition at 300 K is determined by low-energy electron diffraction analysis. The structure consists of missing rows in the top layer of the Cu(001) surface, in which Li atoms are located. The interlayer spacing between the first and second layer of the substrate is contracted by 7% from the bulk value. It is revealed that not only Cu(110) but also Cu(001) undergoes missing-row type restructuring upon alkali-metal adsorption at room temperature.

1. Introduction

We are noticing that the adsorption of atoms and molecules on metals does not simply mean formation of adlayers. For example, it is found from observations of scanning tunneling microscopy (STM) images that the adsorption of oxygen molecules on Cu(110) [1,2] and Ni(110) [3] produces Cu-O or Ni-O chains on the surfaces.

The adsorption of alkali-metal (AM) atoms is not exception. On fcc(110) metal surfaces such as Cu, Ni, Pd and Ag it is established now that the 1x2 structures observed with low-energy electron diffraction (LEED) upon AM adsorption at room temperature do not originate from AM overlayers but from the missing-row type reconstruction on substrate surfaces [4-8]. Recent STM studies for K on Cu(110) clearly demonstrate that a single K atom removes two or three Cu atoms in the top layer and that thus created vacancies grow as missing rows with increasing K coverage [9,10]. The origin of the reconstruction has been discussed theoretically [11,12].

Even on fcc(111), considered to be the most stable surface, recently Schmalz *et al.* have found from surface extended X-ray-absorption fine-structure measurements that Na adatoms substitute surface Al atoms on

Al(111) to form a ($\sqrt{3}$x$\sqrt{3}$)R30° structure at room temperature [13]. Furthermore, Andersen *et al.* have studied the same adsorption system at room temperature with a high-resolution core-level spectroscopy and they have concluded that 2x2 and 2$\sqrt{3}$x2$\sqrt{3}$ structures observed at higher coverages consist of intermixed Na-Al layers [14]. Very recently Stampfl *et al.* have carried out LEED analysis for a similar system of K/Al(111) and they found that the ($\sqrt{3}$x$\sqrt{3}$)R30° structure formed at 300 K is due to substituted K atoms [15].

For fcc(001), a missing-row type reconstruction was suggested for K/Ag(001) [16] and K/Au(001) [17] from LEED observation. Theoretically, the reconstruction of the K/Ag(001) system is supported recently [18]. We have found 2x1, 3x3 and 4x4 LEED patterns for Li adsorption on Cu(001) at 300 K as described in Chapter II [19]. The 2x1 pattern accompanies weak streaky spots, and from their features and behavior we have also proposed that the 2x1 structure is due to the missing-row type restructuring of the Cu(001) surface and that Li atoms are located in the missing-rows. The 3x3 and 4x4 structures are assigned to ordered surface-alloys.

In a course of structure determination of surface materials by LEED analysis, the 2x1 structure of Li/Cu(001) was determined in the present paper; It is the missing-row type restructuring of the top layer of Cu(001) as proposed previously.

2. Experimental

The experiments were carried out in a three-level UHV chamber equipped with standard facilities for surface science [20]. Li was deposited onto the surface from a SAES dispenser at 300 K. The Li coverage, a ratio of the number density of the Li adatoms to that of Cu atoms in the ideal top-layer of Cu(001), was determined by using Li KVV Auger and LEED patterns [19]. During Li deposition the pressure was less than 1.5×10^{-10} Torr. Water in the

chamber is the most active for the Li covered Cu surface [20,21] and its partial pressure was less than $3x10^{-12}$ Torr. After measurement of LEED *I(E)* curves no contamination was detected and the *I(E)* curves did not change. LEED spot intensities were measured with a computer-controlled Auto-LEED system based on the original design of the Erlangen group [22]. LEED *I(E)* curves were taken at normal incidence with an energy range from 20 to 200 eV and with 1 eV step. Sample temperature was 180 K during measurement. Normal-incidence condition was achieved by using the horizontal-beam method [23], in which only two equivalent spots located in the horizontal direction are measured and averaged. Details of the measurement of LEED *I(E)* curves has been described in Chapter III [23].

Standard LEED programs [24] were used to calculate *I(E)* curves for three structure models of the 2x1 structure. Six phase shifts were used to calculate atomic scattering ($l_{max} = 5$). The real part of the inner potential was determined during the course of the theory-experiment fit. Debye temperatures for Cu and Li are 335 K and 480 K, respectively [23].

3. Results and discussion

We have determined the c(2x2) structure formed on Cu(001) upon Li adsorption at 180 K by LEED analysis. It is found that an overlayer of Li atoms sitting on the fourfold hollow sites (coverage 0.5) is preferred with the Cu-Li interlayer spacing of 1.96 Å [23]. The radius of the Li atom is 92% of a Li metallic one. Upon warming the c(2x2) structure converted to the 2x1 structure at about 200 K. However, upon cooling the 2x1 structure did not change to the c(2x2) structure. Similar conversions of surface structures in an irreversible and activated process have been observed commonly for the AM induced reconstructions [4,15-17].

Previously, features and behavior of the streaky spots coexisting with the 2x1 spots led us to propose a structure model for the 2x1 structure as

mentioned above; the top layer of Cu(001) undergoes the missing-row type restructuring upon Li adsorption, and Li atoms are located in the missing rows formed by themselves causing the streaky spots [19]. Top and side views of the proposed structure are depicted in Fig. 1(a). Here, we summarize features and behavior of the weak streaky spots; their periodicity is denoted by $\begin{pmatrix} \frac{1}{2\Theta} & 0 \\ -\frac{1}{4\Theta} & 2 \end{pmatrix}$ in a coverage range of $0.375 \leq \Theta \leq 0.4$ and its unit cell is shown in Fig. 1(a) with solid lines. Li atoms are ordered in each trough (Li chains), while a correlation between the neighboring Li chains is weak. In the troughs the Li-Li distance becomes shorter with increasing coverage. Upon cooling they become distinct spots caused by ordering between the Li chains.

First of all, LEED intensity calculations were performed for the missing-row structure proposed previously [19]. In the present structure model we ignored presence of the Li adatoms as shown in Fig. 1(b) as usually assumed for LEED calculations of the missing-row structures formed on fcc(110) by AM adsorption [6-8]. For fcc(110) surfaces this is due to the largely disordered nature of the AM adatoms, where streaks are developed instead of the streaky spots observed in Li/Cu(001). In the present study we confirmed experimentally that actual LEED *I(E)* curves for the 2x1 structure do not include the contribution of the Li adatoms as shown later. Agreement between theory and experiment was tested by a conventional Pendry R-factor (R_P) analysis[25] that included two integral-order beams of (1 0) and (1 1) and one half-order beam of (0.5 0). The precision of the structure parameters was determined by a sensitive analysis which is based on the steepness of the R_P minimum [25]. For the structure shown in Fig. 1(b), namely the missing-row structure, the R_P is plotted as a function of the interlayer spacing between the first and second layer of Cu(001), d_{12} in Fig. 2. The R_P for the missing row structure has a very steep minimum and its value is 0.168 at d_{12} = 1.68 Å. Around the minimum d_{12} was varied with 0.02 Å step and the step was 0.1 Å

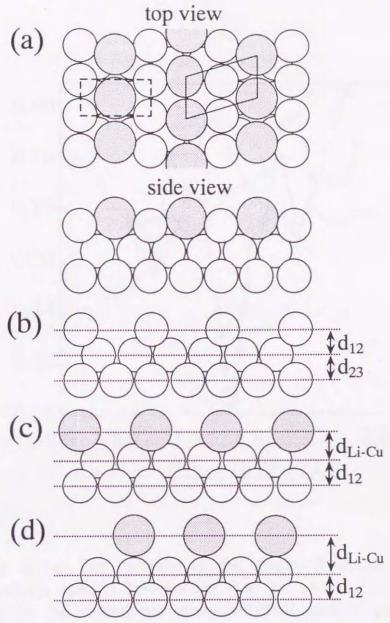

Fig.1. (a) Top and side views of the proposed 2x1 structure formed upon Li adsorption on Cu(001) [19]. Dotted and open circles are Li and Cu atoms, respectively. The solid and broken lines outline $\begin{pmatrix} \frac{1}{2\Theta} & 0 \\ -\frac{1}{4\Theta} & 2 \end{pmatrix}$ and 2x1 unit cells, respectively. Θ means Li coverage. (b) Side view of the missing-row model used for the LEED analysis of the 2x1 structure.The Li adatoms are not considered here for simplicity of calculation. (c) Side view of the Li overlayer adsorbed on the hollow sites. (d) Side view of the Li overlayeradsorbed on the atop sites. In (b)-(d) interlayer spacings are defined.

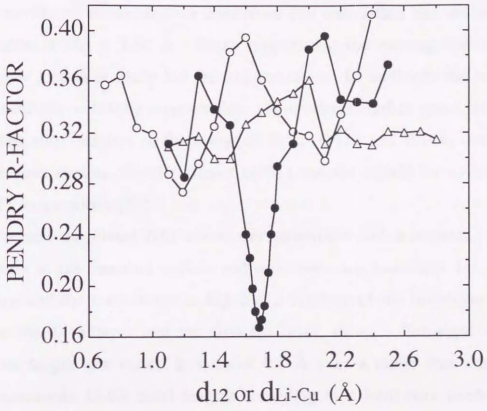

Fig. 2. (a) The variation of the Pendry R-factors with the interlayer spacing between the first and second Cu(001) layer, d_{12}, for the missing-row structure (filled circles) and with the Cu-Li interlayer spacing, $d_{Li\text{-}Cu}$, for the overlayer structures at the hollow (open circles) and atop (triangles) sites.

at other range. d_{12} was varied by approximately ± 40 % of the bulk value, 1.807 Å. As can be clearly seen, there is no other minimum which is so steep and small as that at 1.68 Å. The R_P shown in Fig. 2 is the average of the three beams mentioned above, and we confirmed that each beam has the minimum of R-factor at d_{12} = 1.68 Å. These support that the missing-row structure with d_{12} = 1.68 Å is likely for the 2x1 structure. In addition, the minimum value itself (R_P = 0.168) supports this. This value is rather good, when it is compared with minima of the averaged R_P's, 0.113 and 0.106, obtained in our previous studies for the clean Cu(001) and the c(2x2) Li overlayer on Cu(001), respectively [23].

We have calculated *I(E)* curves for alternative 2x1 structures. The Li overlayers at the fourfold hollow and atop sites are examined for the 2x1 structure, and R_P' s are shown in Fig. 2 as a function of the interlayer spacing between the Li adlayer and the first Cu layer, $d_{Li\text{-}Cu}$. For these sites the adsorbate height was varied in steps of 0.1 Å over a range that was chosen from reasonable Li-Cu bond lengths according to a hard-core model of the atoms. Minima of R_P' s are 0.27 and 0.30 for the hollow and atop sites, respectively, and these are much larger than that for the missing-row structure. Furthermore, they do not have steep minima and each beam has a different minimum position. These clearly indicate that the Li overlayers at the hollow and atop sites are not likely as the 2x1 structure.

Our conclusion from the LEED analysis is that the 2x1 structure originates from the missing-row restructuring. The optimization of this structure was carried out for the interlayer spacing between the second and third Cu layers, d_{23}. The relaxation was varied by ± 6% of the bulk value and we found a minimum of R_P = 0.165 at d_{23} = 1.84 Å in the condition of d_{12} = 1.68 Å. This optimization did not improve R_P considerably. We did not check any lateral displacement because of limitation of the present calculation. The optimum structural parameters for the 2x1 structure together with the

errors are the following; d_{12} = 1.68±0.05 Å and d_{23} = 1.84±0.07 Å. The errors were estimated from the total energy range ΔE = 400 eV using the variance of R_P-factor $\Delta R = R(8V_{oi}/\Delta E)^{1/2}$, where R is the minimum R_P-factor achieved [25] and the imaginary part of the inner potential V_{oi} was chosen to be proportional to $E^{1/3}$. Because of the rather small value of ΔE the error limits are rather high (ΔR = 0.05). A comparison of the experimental *I(E)* curves with those calculated for the optimum geometry is shown in Fig. 3, from which a very good agreement is evident.

In the theoretical calculation of the missing-row structure, we ignored the presence of Li adatoms. In Fig. 4, curves (a) and (b) are experimental *I(E)* curves for (0.5 0) beams obtained from the Li adsorbed surfaces at coverages of 0.3 and 0.4, respectively. At the coverage of 0.3 LEED did not exhibit the streaky spots, while it showed the brightest streaky spots at 0.4. The (0.5 0) spots are degenerate for the 2x1 and the streaky spots [19]. Therefore, the *I(E)* curve (b) would include a contribution from the Li adatoms, and the curves (a) and (b) would be different. However, the *I(E)* curves at the two different coverages are almost the same except for their absolute intensities. The contribution from the Li adatoms seems to be negligible.

Having determined the 2x1 structure, the next problem is where the Li atoms are located. There are two possible locations for the Li adatoms, namely troughs and ridges. Basically for this we need to carry out LEED analysis of the streaky spots, because they are originated from the Li adatoms [19]. Unfortunately, their intensities are weak and energy-range where we can observe them are very limited. Therefore, it is difficult to get their *I(E)* curves, and consequently we cannot determine position of the Li adatoms by LEED analysis. However, we can conclude that the most provable Li site is troughs by considering features and behavior of streaky spots mentioned

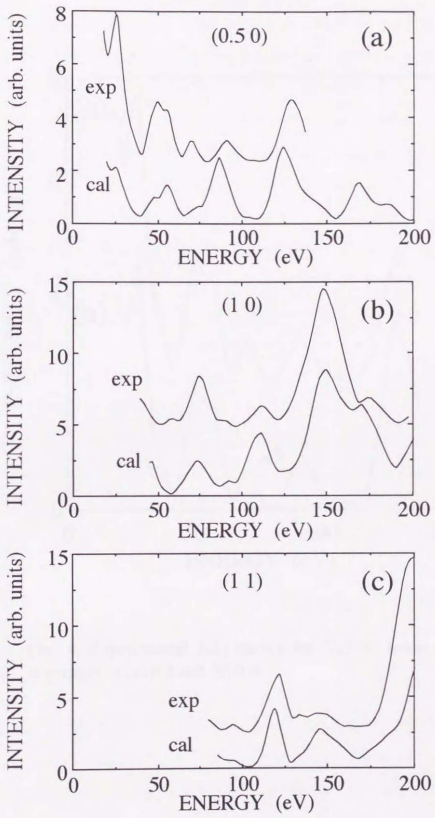

Fig. 3. *I(E)* curves as measured (exp) and calculated (cal) for the best fit (the missing row structure with d_{12} = 1.68 Å and d_{23} = 1.84 Å).

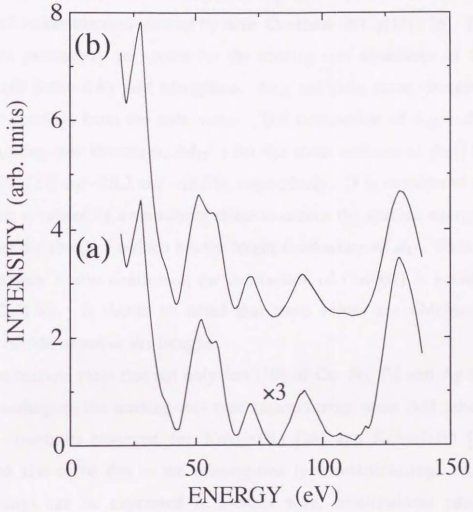

Fig. 4. Experimental *I(E)* curves for (0.5 0) beam at Li coverages of (a) 0.3 and (b) 0.4.

above. High coordination-number sites are preferred for AM adatoms theoretically [11] and this supports the trough sites in the present system.

Finally, we would like to compare the present result with that obtained for the 1x2 reconstruction induced by K or Cs atoms on Cu(110) [8]. In Table 1 structure parameters are shown for the missing-row structures of Cu(001) and Cu(110) induced by AM adsorption. Δd_{12} and Δd_{23} mean changes of the interlayer spacings from the bulk value. The contraction of d_{12} is common for the missing-row structures; Δd_{12}' s for the clean surfaces of Au(110) [26] and Pt(110) [27] are –20.3 and –18.3%, respectively. It is considered that the contraction is caused by a smoothing effect to reduce the surface energy. It is known that the rougher surface has the larger contraction of d_{12}. From Table 1 this tendency is also confirmed; the contraction of Cu(001) is smaller than that of Cu(110). It should be noted that these values are obtained under existence of AM atoms in the troughs.

It has become clear that not only fcc(110) of Cu, Ni, Pd and Ag but also Cu(001) undergoes the missing-row type restructuring upon AM adsorption. The 2x1 structures observed for K/Ag(001) [16] and K/Au(001) [17] are considered also to be due to the missing-row type restructuring. All these restructurings can be expressed in another way, substitutional adsorption. Furthermore, on Al(111) Na or K atoms substitute the substrate surface atoms also [13,15]. Therefore, the occurrence of the substitutional adsorption on some fcc metal surfaces of (001), (110) and (111) leads us to suggest that the substitutional adsorption takes place on other planes also. It should be noted, however, that K adatoms do not induce the substitution on Cu(001) at room temperature [28]. Therefore, the substitutional adsorption of AM atoms is dependent on the combination of AM and substrate surface and temperature.

Table 1

Optimum parameters for the missing-row structures induced by AM adsorption on Cu(110) and Cu(001).

	Δd_{12}	Δd_{23}	Ref.
Cu(110)	−11%	0%	8
Cu(001)	−7 ± 3%	+2 ± 4%	This work

4. Conclusion

LEED analysis provides a model for the 2x1 structure on Cu(001) induced by Li deposition at 300 K. The missing-row structure is preferred and optimum structure parameters are d_{12} = 1.68±0.05 Å and d_{23} = 1.84±0.07 Å. This is the first confirmation of the missing-row structure formed on fcc(001) upon AM adsorption. It is evident that not only fcc(110) but also fcc(001) metal surface undergoes the missing-row type restructuring upon AM adsorption.

References

[1] D. J. Coulman, J. Wintterlin, R. J. Behm and G. Ertl, Phys. Rev. Lett. **64** (1990) 1761.

[2] F. Jensen, F. Besenbacher, E. Lægsgaard and I. Stensgaard, Phys. Rev. **B 41** (1990) 10233.

[3] L. Eierdal, F. Besenbacher, E. Lægsgaard and I. Stensgaard, Ultramicroscopy, **42-44** (1992) 505.

[4] R. J. Behm, in: Physics and Chemistry of Alkali Metal Adsorption, Eds. by H. P. Bonzel, A. M. Bradshaw and G. Ertl (Elsevier, Amsterdam, 1989) p. 111.

[5] C. J. Barnes, M. Lindroos, D. J. Holmes and D. A. King, in Ref. 4, p. 129.

[6] C. J. Barnes, M. Lindroos and D. A. King, Surf. Sci. **201** (1988) 108.

[7] C. J. Barnes, M. Lindroos, D. J. Holmes and D. A. King, Surf. Sci. **219** (1989) 143.

[8] Z. P. Hu, B. C. Pan, W. C. Fan and A. Ignatiev, Phys. Rev. **B41** (1990) 9692.

[9] R. Schuster, J. V. Barth, G. Ertl and R. J. Behm, Phys. Rev. **B 44** (1991) 13689.

[10] R. Schuster, J. V. Barth, G. Ertl and R. J. Behm, Surf. Sci. **247** (1991) L229.

[11] K.W. Jacobsen and J. K. Nϕrskov, Phys. Rev. Lett. **60** (1988) 2496.

[12] C.L. Fu and K.M. Ho, Phys. Rev. Lett. **63** (1989) 1617.

[13] A. Schmalz, S. Aminpirooz, L. Becker, J. Haase, J. Neugebauer, M. Scheffler, D. R. Batchelor, D. L. Adams and E. Bϕgh, Phys. Rev. Lett. **67** (1991) 2163.

[14] J. N. Andersen, M. Qvarford, R. Nyholm, J. F. van Acker and E. Lundgren, Phys. Rev. Lett. **68** (1992) 94.

[15] C. Stampfl, M. Scheffler, H. Over, J. Burchhardt, M. Nielsen, D. L. Adams and W. Moritz, Phys. Rev. Lett. **69** (1992) 1532.

[16] M. Okada, H. Tochihara and Y. Murata, Phys. Rev. **B 43** (1991) 1411; Surf. Sci. **245** (1991) 380.

[17] M. Okada, H. Iwai, R. Klauser and Y. Murata, J. Phys.: Condens. Matter **4** (1992) L593.

[18] O.B. Christensen and K.W. Jacobsen, Phys. Rev. **B 45** (1992) 6893.

[19] H. Tochihara and S. Mizuno, Surf. Sci. **279** (1992) 89.

[20] S. Mizuno, H. Tochihara, T. Kadowaki, H. Minagawa, K. Hayakawa, I. Toyoshima and C. Oshima, Surf. Sci. **264** (1992) 103.

[21] H. Tochihara and S. Mizuno, Chem Phys. Lett. **194** (1992) 51.

[22] K. Müller and K. Heinz, Springer Series in Surface Sciences, Vol. **2** (Springer, Berlin, 1985) p. 105.

[23] S. Mizuno, H. Tochihara and T. Kawamura, Surf. Sci. **293** (1993) 239.

[24] M. A. Van Hove and S. Y. Tong, Springer Series in Chemical Physics, Vol. **2**, Surface Crystallography by LEED (Springer, Berlin, 1979).

[25] J. B. Pendry, J. Phys. **C 13** (1980) 937.

[26] W. Moritz and D. Wolf, Surf. Sci. **163** (1985) L655.

[27] E.C. Sowa, M.A. Van Hove and D.L. Adams, Surf. Sci. **199** (1988) 174.

[28] T. Aruga. H. Tochihara and Y. Murata, Surf. Sci. **158** (1985) 490.

VI. Geometries of Li induced structures on Cu(001): ARUPS studies

Superstructures of c(2x2) and 2x1 are formed on Cu(001) initially with increasing Li coverage at sample temperatures of 180 and 300 K respectively, and these structures have been determined by low-energy electron diffraction intensity analysis. Li adatoms are located on fourfold hollow sites for the c(2x2) structure and that the 2x1 structure is caused by a missing-row-type restructuring of the top layer of Cu(001). The Tamm-type surface state of the Cu(001) surface is monitored as a function of Li coverage at 180 and 300 K with angle-resolved ultraviolet photoelectron spectroscopy at $\bar{M}$ point. Different behaviors of the surface state at 180 and 300 K at low coverages are discussed in connection with different geometries of Li adatoms formed at the two temperatures.

1. Introduction

It is known that alkali-metal atoms induce a reconstruction on fcc(110) surfaces such as Ni, Pd, Cu and Ag at room temperature [1, 2]. Low-energy electron diffraction (LEED) exhibits 1x2 patterns for these systems, and LEED intensity analysis for Cs/Ag(110) [3] and K/Cu(110) [4] confirmed that the 1x2 structures are caused by a missing-row-type reconstruction. A recent STM study by Schuster *et al.* for K/Cu(110) has clearly demonstrated that the interaction of an alkali-metal adatom and the substrate surface is very local at low coverages [5].

On the other hand, on fcc(001) metal surfaces quasihexagonals of alkali-metal overlayers are formed usually [6]. However, non-quasihexagonal structures have been observed by using LEED; 2x1 and 3x1 for K/Ag(001) at 315-335K [7] and 2x1, 3x3 and 4x4 for Li/Cu(001) at 300 K [8]. It has been

considered that all these structures are related to restructurings of the substrate surfaces induced by alkali-metal atoms.

The 2x1 structure of Li/Cu(001) accompanies weak streaky spots [8]. Their features and behaviors are very similar to those observed for systems of Cs or K adsorption on Ni(110) [9] or Cu(110) [10] at room temperature, and this has led to a structure model for the 2x1 structure; the Cu(001) surface undergoes a missing-row-type restructuring upon Li adsorption. Li adatoms are located in missing rows formed by themselves as depicted in Fig. 1(b) [8]. This missing-row structure is very similar to those for fcc(110) metal surfaces. On the other hand, at 180 K the superstructure observed first is c(2x2) with increasing Li coverage, then complicated structures appear successively [8,11]. Such differences of structures between 300 and 180 K should be reflected in the electronic and other properties. Therefore it is valuable to study the differences of properties by using conventional techniques. In this chapter the initial stages of Li adsorptions are studied with angle-resolved ultraviolet photoelectron spectroscopy (ARUPS).

2. Experiments

The experiments were carried out in a three-level UHV chamber equipped with ARUPS, LEED, Auger electron spectroscopy, X-ray photoelectron spectroscopy and high-resolution electron energy-loss spectroscopy [12]. Li was deposited onto the surface from a SAES dispenser. During Li deposition the pressure was less than 1.5×10^{-10} Torr. Only water in the chamber is active for the Li covered Cu surface [12,13] and its partial pressure was less than 3×10^{-12} Torr.

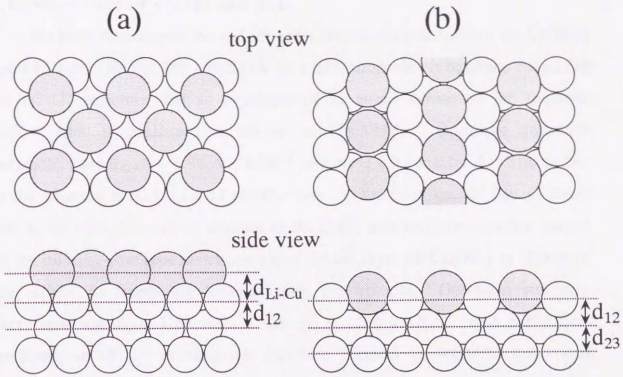

Fig.1. Top and side views of (a) the c(2x2) Li-overlayer adsorbed on fourfold hollow sites of Cu(001) and (b) the 2x1 structure due to substitutional adsorption of Li adatoms with the surface Cu atoms on Cu(001). Dotted and open circles are Li and Cu atoms, respectively.

3. Results and discussion

3.1. Structures of c(2x2) and 2x1

We have determined the c(2x2) and (2x1) structures formed on Cu(001) upon Li adsorption at 180 and 300 K by LEED analysis. It has been found for the c(2x2) structure that an overlayer of Li atoms sitting on the fourfold hollow sites is preferred as shown in Fig. 1(a). Optimum structure parameters are $d_{Li\text{-}Cu}$ = 1.96 Å ± 0.08 Å and d_{12} = 1.81 ± 0.04 Å. The radius of the Li atom is 92% of a Li metallic one. It has been known that at about 200 K the c(2x2) structure changes to the (2x1) structure irreversibly caused by the missing-row type restructuring of the top layer of Cu(001) as shown in Fig. 1(b). Li atoms are located inside the troughs. Optimum structure parameters are d_{12} = 1.68±0.05 Å and d_{23} = 1.84±0.07 Å. This is the first confirmation of the missing-row structure formed on fcc(001) upon AM adsorption.

3.2. The coordination number of Li adatoms

ARUPS has been used to study electronic properties of the two different structures induced by Li adsorption at 180 and 300 K. However, we could not detect Li induced features in ARUPS spectra from the two surfaces. Instead we notice that the Tamm-type surface state of the Cu(001) surface is well seen at $\overline{M}$ point in the surface Brillouin zone with ARUPS [14, 15]. The Tamm states arise from the increased Coulomb repulsion at the surface due to excess *s*, *p*-electron density [16]. At $\overline{M}$ point, the M_2 Tamm state originated from the 3*d* level of the surface Cu atoms is pushed out of the bulk 3*d* band by 200 meV, being observed in an ARUPS spectrum as shown in Fig. 2. We have studied behaviors of the surface state with increasing Li coverage at 180 and 300 K. At both temperatures the Tamm state shifts to high binding-energy side as shown in Fig. 3 [17] and its intensity decreases linearly at low coverages as a function of Li coverage, θ as shown in Fig. 4 [18]. Fortunately, we have found a considerable difference in the decrease of the

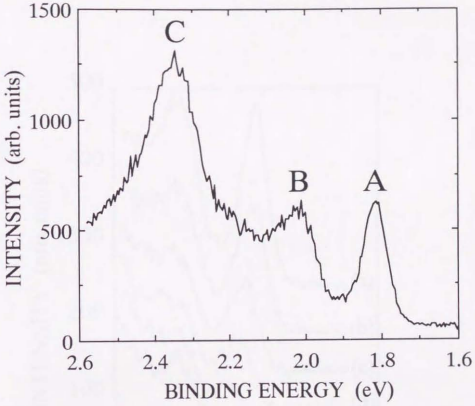

Fig. 2. An ARUPS spectrum of the clean Cu(001) surface at the $\bar{M}$ point with unpolarized He I. (A) The Tamm-type surface state; (B) and (C) bulk 3d states.

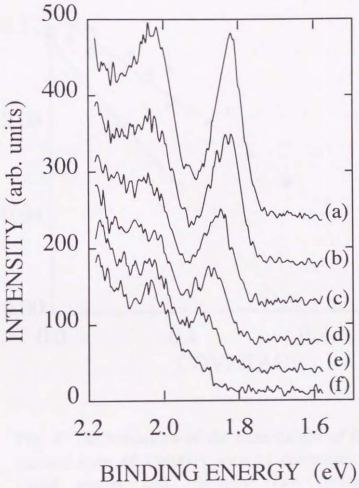

Fig. 3. ARUPS spectra for the surface state of the Li/Cu(001) at 300 K. (a)-(f) θ_{Li} = 0, 0.05, 0.1, 0.15, 0.2, 0.25.

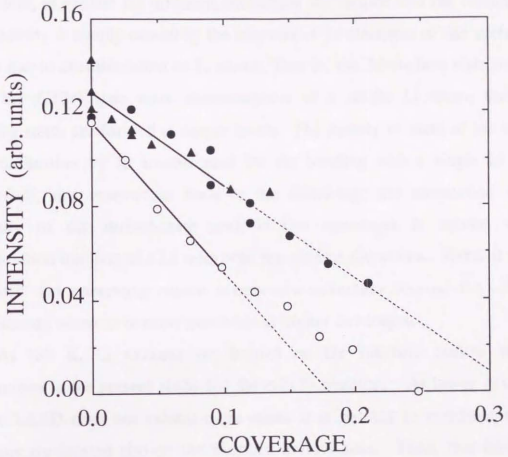

Fig. 4. The variations of the peak-height of the Tamm-type surface state of Cu(001) with Li coverage, θ, at 180 K (solid circles and triangles; two different runs of experiment) and at 300 K (open circles). Straight solid lines ($\theta \leq 0.1$) are used to obtain the removal numbers. See text.

surface state intensity; the surface state attenuates at 300 K much more rapidly that that does at 180 K at low coverages.

Here, to explain the different attenuation we assume that the reduction of the intensity is simply caused by the removal of 3*d* electrons of the surface Cu atoms due to chemisorption of Li atoms. That is, the 3*d* surface state interacts with the Li(2*s*) state upon chemisorption of a single Li atom, then new bonding states are formed at deeper levels. The density of state of the surface state diminishes by an amount used for the bonding with a single Li atom. Therefore, this assumption leads to the following; the attenuation of the intensity of the surface-state peak at low coverages is related to the coordination number of a Li atom with the surface Cu atoms. Here, it should be noted that interesting region is only low coverages because the effect of neighboring adatoms become inevitable at higher coverages.

At 180 K, Li adatoms are located on the fourfold hollow sites as determined in the present study for the c(2x2) structure. At lower coverages where LEED does not exhibit extra spots, it is natural to conclude that Li adatoms are located also on the fourfold hollow sites. Then, this leads to a suggestion that a single Li adatom removes the density of state of the surface state contributed from four Cu atoms (*i.e.*, the coordination number four) at low coverages.

On the other hand, at 300 K Li adatoms are located in troughs formed by themselves for the 2x1 structure. Since there is no STM observation for Li/Cu(001) at 300 K yet, we borrow results of STM observation for the K/Cu(110) system which shows similar restructuring as mentioned above [5]. According to that STM study, a single K atom removes two or three surface Cu atoms and in the vacancy the K adatom is located. In the present system we suppose that a single Li atom removes one or two Cu atoms at low coverages, because Li is smaller than K and larger than Cu. Then, at low coverages a single Li atom removes the density of state (the surface state)

contributed from at least five or six surface Cu atoms, because one Li atom removes one or two Cu atoms out of the Cu(001) surface and bonds with at least four Cu atoms in the top layer. This corresponds to the coordination number of 5 or 6, but as a matter of fact this is not the coordination number. Henceforth we use a term of the removal number instead. The removal number means the number of substrate surface-atoms removed by and bonded with a single adatom.

From straight lines indicated in Fig. 4, the removal numbers are determined to be 3±1 and 6 for 180 and 300 K at low coverages ($\theta \leq 0.1$), respectively. The result is in good agreement with the expected values above. Therefore, it is likely that the attenuation of the surface state due to Li adsorption is directly related to the removal number of a Li atom at low coverages.

4. Conclusion

Behaviors of the Tamm-type surface state of the Cu(001) surface is monitored as a function of Li coverage at 180 and 300 K with ARUPS at $\bar{M}$ point. The Tamm state shifts to high binding-energy side and its intensity decreases linearly at low coverages as a function of Li coverage. The removal numbers, which has defined in previous section, are determined to be 3±1 and 6 for 180 and 300 K from the initial slope of the Fig. 4. The removal numbers are consistent with the local geometries of Li adatoms.

Reference

[1] R.J. Behm, in: Physics and Chemistry of Alkali Metal Adsorption, Eds. by H.P. Bonzel, A.M. Bradshaw and G. Ertl (Elsevier, Amsterdam, 1989) p. 111.

[2] C.J. Barnes, M. Lindroos, D.J. Holmes and D.A. King, in Ref. [1], p. 129.

[3] C.J. Barnes, M. Lindroos, D.J. Holmes and D.A. King, Surf. Sci. **219** (1989) 143.

[4] Z.P. Hu, B.C. Pan, W.C. Fan and A. Ignatiev, Phys. Rev. **B41** (1990) 9692.

[5] R. Schuster, J.V. Barth, G. Ertl and R.J. Behm, Phys. Rev. **B44** (1991) 13689; Surf. Sci. **247** (1991) L229.

[6] K. Müller, G. Besold and K. Heinz, in Ref. [1], p. 65.

[7] M. Okada, H. Tochihara and Y. Murata, Phys. Rev. **B43** (1991) 1411; Surf. Sci. **245** (1991) 380.

[8] H. Tochihara and S. Mizuno, Surf. Sci. **292** (1992) L811.

[9] R.J. Behm, D.K. Flynn, K.D. Jamison, G. Ertl and P. A. Thiel, Phys. Rev. **B36** (1987) 9267.

[10] W.C. Fan and A. Ignatiev, Phys. Rev. **B38** (1988) 366.

[11] S. Mizuno and H. Tochihara, to be published.

[12] S. Mizuno, H. Tochihara, T. Kadowaki, H. Minagawa, K. Hayakawa, I. Toyoshima and C. Oshima, Surf. Sci. **264** (1992) 103.

[13] H. Tochihara and S. Mizuno, Chem Phys. Lett. **194** (1992) 51.

[14] P. Heimann, J. Hermanson, H. Miosga and H. Neddermeyer, Phys. Rev. Lett. **42** (1979) 1782; Phys. Rev. **B20** (1979) 3059.

[15] P.L. Wincott, D.S.-L. Law, N.B. Brookes, B. Pearce and G. Thornton, Surf. Sci. **178** (1986) 300.

[16] A. Euceda, D.M. Bylander, L. Kleinman and K. Mednick, Phys. Rev. **B27** (1983) 659.

[17] H. Tochihara and S. Mizuno, to be published.

[18] θ=1 corresponds to 1 Li atom per 1 Cu atom in the ideal topmost surface. See Ref. 8 for determination of θ.

VII. Alkali-metal adsorption on dissimilar alkali-metal monolayers preadsorbed on Cu(001): Li on Na and Na on Li

A new adsorption system of metal-on-metal growth is presented. The adsorption of alkali-metal atoms on monolayers of dissimilar alkali-metals preadsorbed on the Cu(001) surface has been studied for the first time by Auger electron spectroscopy, work-function change and low-energy electron diffraction intensity analysis. We have examined the following three adsorption systems on Cu(001) at 180 K; Na on a full monolayer of Li, Li on a full monolayer of Na, and Na on a submonolayer of Li, namely the c(2x2) structure of Li adatoms. It is found that simple overlayer formation of Na takes place on the full Li monolayer while Li atoms substitute Na adatoms for Li adsorption on the full Na monolayer. For adsorption of Na on the Li-c(2x2) structure whose coverage is 5/8 of the full Li monolayer, it is found that Na atoms compress the Li adlayer to become denser monolayers. The Na atoms do not intermix with Li adatoms and form islands of the c(2x2) structure on Cu(001).

1. Introduction

The adsorption of alkali-metal atoms on transition or noble metal surfaces has been studied experimentally and theoretically for many years [1]. One of the most interesting features of the alkali-metal adsorption on the metals is a drastic changes of surface structures and properties during monolayer formation, typically seen in work function change [1]. In these changes we have an implicit understanding that alkali-metal atoms form overlayers on metals. Recent studies, however, have revealed that reconstructions of substrate take place on some metal planes upon alkali-metal adsorption at room temperature. For example, on fcc(110) metal surfaces of Ag, Cu, Ni and Pd, it has been known that alkali-metal atoms induce a

missing-row type reconstruction of substrate surfaces at 300 K [2]. On fcc(001) also, the missing-row type reconstructions in the top layer are found for K/Ag(001) [3], K/Au(001) [4] and Li/Cu(001) [5] at 300 K. Even on fcc(111), a substituted top substrate layer of the $(\sqrt{3}x\sqrt{3})R30^\circ$ structure is determined for K/Al(111) by low-energy electron diffraction (LEED) analysis [6]. Following the missing-row type reconstruction or substitutional adsorption, surface alloy formation between substrate and alkali-metal atoms takes place with increase of coverage for the adsorption systems above. It is noted that temperature necessary for these processes is higher than ~200 K [2-6]. On the other hand, at temperatures lower than 200 K, alkali-metal overlayers are formed instead.

As mentioned above, on some transition and noble metal surfaces, a variety of growth modes of alkali-metal atoms has been found. It is interesting to use an alkali-metal as a substrate to be adsorbed by dissimilar alkali-metal atoms. Since the adsorbate and substrate belong to an alkali-metal group, interaction between them would be very different from that between alkali-metal and transition or noble metals. Consequently, we may find a new type of growth mode different from those already known.

However, it is difficult to make single crystals of alkali-metals. Therefore, instead of a bulk crystal, we use a monolayer of alkali-metals on Cu(001). Fortunately, monolayers of alkali-metals on Cu(001) exhibit well ordered two-dimensional lattices at low temperatures [7-11]. Therefore, we can study structures and growth modes due to alkali-metal adsorption on dissimilar alkali-metal monolayers by using LEED. To date, this adsorption system, i. e., alkali-metal on alkali-metal, has not been performed yet as far as we know.

In this paper, we have studied the following three adsorption systems at 180 K: (1) Na on a full monolayer of Li on Cu(001), (2) Li on a full monolayer of Na on Cu(001), and (3) Na on a submonolayer of Li on

Cu(001). In the three adsorption systems, we have found (1) simple overlayer formation of Na, (2) substitution of Na adatom by Li, and (3) compression of Li adlayer and phase separation into Li and Na domains, respectively. Following Sec. II (experiment and calculation), detailed results of the three adsorption systems above studied by LEED, Auger electron spectroscopy (AES) and work function change are described in Sec. III with some discussions. Summaries are reviewed in Sec. IV.

2. Experiment and calculation

Experiments were carried out in a three-level UHV chamber equipped with various probes [12]. LEED and AES were principal tools in the present study. In particular, AES of Li KVV and Na LVV transitions played a crucial role in alkali-metal on alkali-metal systems. Work function change was measured by using a derivative mode of the AES system, and the cutoff of secondary electron emission was used with sample bias. The Cu(001) surface was cleaned with a procedure mentioned below. LEED spots from the clean surface were sharp, and the background was satisfactorily low. Alkali-metals were deposited onto the surface from SAES dispensers (SAES Getters) at 180 K. LEED spot intensities were measured with a computer-controlled Auto-LEED system for surface structure determination. LEED intensity-energy curves, $I(E)$, were taken with incident-energy range from 20 to 200 eV and with 1 eV step. Normal-incidence condition was achieved approximately by using the horizontal-beam method [13], in which only two equivalent spots located in the horizontal direction are averaged. It should be noted that all experiments were carried out at 180 K. In the present paper, the coverage of alkali-metal atoms is always defined as the ratio of the number density of alkali-metal atoms with respect to that of copper atoms in the ideal Cu(001) surface.

Special cares were taken in the present experiment for the following two points. First, we paid attention to pressure in the chamber, because alkali-metal deposited Cu(001) surfaces are easily contaminated by residual gases. Since water in the chamber is the most active species for alkali-metal covered Cu surfaces [12,14], a liquid-nitrogen shroud was used to remove the water. Then, the partial pressure of water was less than $3x10^{-12}$ Torr during experiments. The total and CO partial pressures during experiments were $1.0x10^{-10}$ and $3x10^{-12}$ Torr, respectively. Most of the residual gas was hydrogen, and oxygen was not found. We confirmed by using high-resolution electron energy loss spectroscopy (HREELS) that hydrogen is not adsorbed on alkali-metal deposited Cu(001) surfaces at 180 K. During alkali-metal deposition the pressure rose to $1.5x10^{-10}$ Torr, and the pressure rise was due to hydrogen with small increase of CO. After an experiment of alkali-metal adsorption on a dissimilar alkali-metal monolayer, we did not detect hydroxide, oxide, CO and other contaminants by HREELS, AES, X-ray photoelectron spectroscopy, ultra-violet photoelectron spectroscopy and work function change. It is noted also that no residual gas is adsorbed on the clean Cu(001) surface at 180 K. This keeps the surface clean until alkali-metal atoms are deposited.

Second, we paid attention to cleaning of the Li deposited surface after an experiment, because Li atoms interdiffuse into bulk at high temperatures. The Li adsorbed surface was cleaned by Ar ion sputtering first then annealed up to 600°C. With this procedure, we always got a clean surface. When we changed the order of sputtering and annealing, we got a contaminated surface due to segregated and reacted Li atoms. At room temperature as shown in our previous studies [5], Li atoms replace copper surface atoms and make surface alloys. It was found by using AES and HREELS for electronic excitations that Li atoms stay in the surface region at 300 K. At 180 K, where the

experiments were performed, Li atoms do not replace substrate atoms and do not interdiffuse into bulk.

Standard LEED programs [15] were used to calculate *I(E)* curves. Six phase shifts were used to calculate atomic scattering (l_{max} = 5). The real part of the inner potential is determined during the course of the theory-experiment fit. The Debye temperature of Cu is 335 K. The Debye temperatures of the Li and Na overlayers are 480 [7] and 160 K [16], respectively.

3 . Results and discussion

3.1. Li or Na atom adsorption on Cu(001)

Here we briefly summarize structures of Li or Na adsorption on Cu(001) observed with LEED in order to help understanding results of alkali-metal on alkali-metal systems. In addition, we describe Auger transitions of Li and Na adatoms on copper surfaces, because they play an important role in the alkali-metal on alkali-metal systems as demonstrated in the main part of this paper.

3.1.1. LEED observations

In Fig. 1, sequential changes of LEED patterns for Li or Na adsorption on Cu(001) at 180 K are summarized with increase of coverages. Similar adsorption systems, K [8,9] or Cs [10,11] on Cu(001), have been studied previously. The c(2x2) structures, observed for both Li [7] and Na [16] adsorption systems, have been determined by means of LEED intensity analysis. It was found that Li or Na adatoms occupy the four-fold hollow sites of the Cu(001) surface and that the coverages are 0.5. The Na-c(2x2) structure corresponds to the full monolayer, while the Li-c(2x2) structure is a submonolayer whose coverage is 5/8 of the full monolayer as seen in Fig. 1. Complicated structures at high Li coverages are due to overlayers, and we will propose these structure models elsewhere [17].

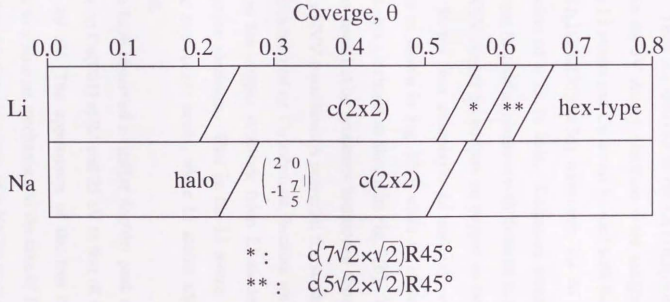

Fig. 1. Surface-structure changes for adsorption systems of Li/Cu(001) and Na/Cu(001) at 180 K as a function of alkali-metal coverage, θ.

3.1.2. AES of Li KVV and Na LVV

Previously, we found two Auger peaks of Li KVV at 46 and 49 eV for the Li deposited Cu(001) surfaces [5]. We assigned that the 49 eV Auger electrons come from Li 2s valence electrons in the deexcitation process of a Li 1s hole. They are denoted as the Li(1s)Li(2s)Li(2s) transition. On the other hand, the 46 eV Auger electrons were assigned as an interatomic transition between Li atoms and Cu atoms bonded with the Li atoms. They are denoted as the Li(1s)Cu(3d)Cu(3d) transition; Cu 3d electrons are involved in the deexcitation of a Li 1s hole. Estimated kinetic energies of the two Auger peaks were in good agreement with those of our experiments [5]. A feature of the Li KVV Auger transitions on copper surfaces is schematically depicted in Fig. 2. In the first monolayer Li adatoms emit both 49 and 46 eV Auger electrons as shown in Fig. 2(a), while Li atoms in the second layer emit only 49 eV Auger electrons as shown in Fig. 2(b). This difference comes from the different deexcitation processes mentioned above. It should be noted that AES of the Li KVV transitions is powerful for studies of Li atom adsorption on Na atoms preadsorbed on Cu substrate, because we can easily distinguish Li atoms sitting on the copper substrate from Li atoms sitting on Na adatoms by Li KVV Auger electrons. That is, the Li atoms sitting on the copper substrate have the two Auger peaks, while Li atoms adsorbed on Na atoms have only one peak.

We have observed a similar doublet peak of LVV Auger electrons of Na adatoms on Cu(001) at 22 and 25 eV to that of the Li KVV Auger electrons at 46 and 49 eV. The appearance of the two Na LVV Auger peaks can be ascribed to a similar mechanism to the case of Li adatoms on Cu(001). In Fig. 3, two deexcitation processes of a Na 2p core hole are illustrated. We have assigned that the 25 and 22 eV peaks are denoted as the Na(2p)Na(3s)Na(3s) and Na(2p)Cu(3d)Cu(3d) transitions, respectively. We estimate kinetic energies of the former and latter Auger electrons to be 25.3 and 21.1 eV,

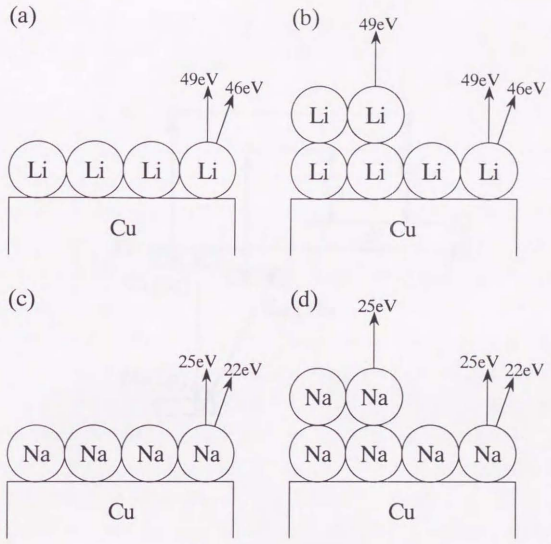

Fig. 2. Illustrations of the characteristic Auger electron emissions from the first and the second layer of Li and Na adatoms on Cu surface. The Li KVV Auger electrons having kinetic energies 49 and 46 eV are denoted as the Li(1s)Li(2s)Li(2s) and Li(1s)Cu(3d)Cu(3d) transitions, respectively. The Na LVV Auger electrons at 25 and 22 eV are termed as the Na(2p)Na(3s)Na(3s) and Na(2p)Cu(3d)Cu(3d) transitions, respectively. (a) Li monolayer on copper substrate (b) Li double layer on Cu (c) Na monolayer on Cu (d) Na double layer on Cu.

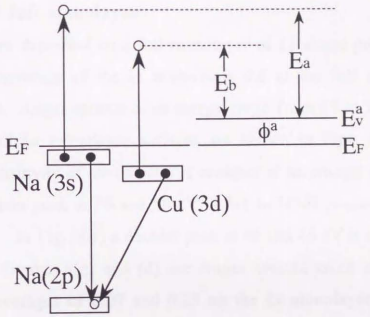

Fig. 3. Schematic diagram for two possible transitions of the Na LVV Auger. E_a and E_b are kinetic energies measured by the analyzer for transitions Na(2p)Na(3s)Na(3s) and Na(2p)Cu(3d)Cu(3d), respectively. E_F is the Fermi level. E_V^a is the vacuum level for the analyzer. ϕ^a is the work function of the analyzer.

respectively and these are in good agreement with our typical peak energies, 25.2 and 22.2 eV. As shown in Fig. 2(c), at the first monolayer Na adatoms emit both 25 and 22 eV Auger electrons, while Na atoms in the second layer emit only 25 eV Auger electrons as shown in Fig. 2(d).

3.2. Na on Li full monolayer

Na atoms are deposited on a full monolayer of Li atoms preadsorbed on Cu(001). The coverage of the Li adatoms is 0.8 at the full monolayer as mentioned above. Auger spectra in an energy range from 15 to 70 eV for the clean and the full Li monolayer surfaces are shown in Figs. 4(a) and (b), respectively. Sensitivity of the detector is changed at an energy of 30 eV. In Fig. 4(a), a doublet peak at 58 and 56 eV is due to MNN Auger electrons of copper substrate. In Fig. 4(b) a doublet peak at 49 and 46 eV is seen for a full Li monolayer. Figures 4(c) and (d) are Auger spectra taken after Na atom deposition of coverages of 0.07 and 0.25 on the Li monolayer on Cu(001), respectively. In these spectra, a single peak of Na Auger appears at 25 eV. Intensities of both Li Auger peaks decrease when Na atoms are deposited on the Li covered surface as clearly seen in Fig. 4(d), and which suggests that the Na atoms cover up the Li monolayer. A clearer evidence for formation of the Na overlayer on the Li covered surface is that the Na Auger peak at 22 eV do not appear during Na adsorption, as seen in Figs. 4(c) and (d). Suppose that Na atoms substitute Li atoms preadsorbed on Cu(001), then the 22 eV Auger peak should be observed because the Na atoms make bonds with the copper substrate.

Na overlayer formation on the Li full monolayer preadsorbed on Cu(001) is consistent with a result of work function change measurement. The work function change is plotted as a function of Li and Na coverages in Fig. 5. In the left-hand side panel of Fig. 5, a typical work function change for alkali-metal adsorption systems is observed with increasing Li coverage on

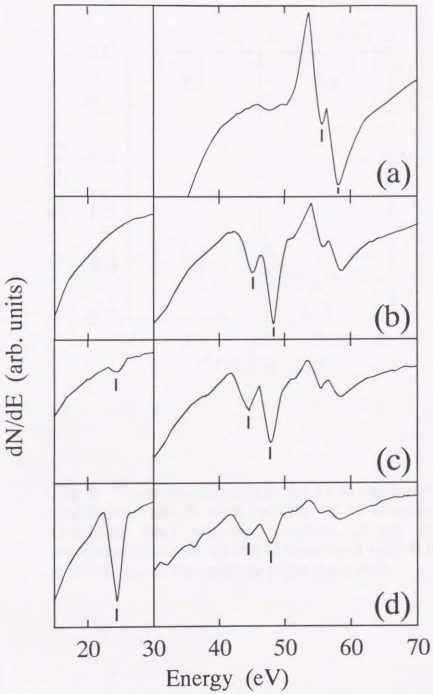

Fig. 4. Na LVV Auger spectra (left-hand side) and Li KVV Auger spectra (right-hand side) at 180 K. (a) Clean Cu(001). (b) A full monolayer of Li on Cu(001), θ_{Li}=0.8. (c) Na is deposited onto the full Li monolayer on Cu(001), θ_{Na}=0.07. (d) same as (c) but θ_{Na}=0.25.

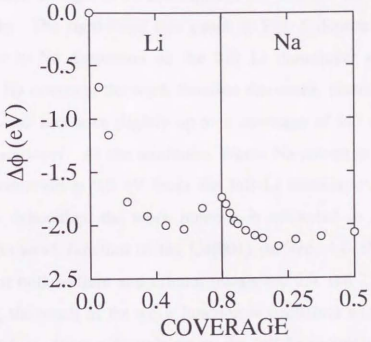

Fig. 5. Work-function change for Li adsorption on Cu(001) at 180 K with increase of Li coverage (left-hand side) and work-function change for adsorption of Na on the full Li monolayer (θ_{Li}=0.8) at 180 K versus Na coverage (right-hand side).

Cu(001); The work function reaches a minimum at Li coverage of 0.5 and recovers slightly up to the monolayer completion at coverage of 0.8. The work function changes at Li coverages of 0.5 and 0.8 are –2.1 and –1.7 eV, respectively. The right-hand side panel of Fig. 5 depicts the work function change due to Na deposition on the full Li monolayer on Cu(001). With increasing Na coverage the work function decreases, passes through a shallow minimum, and increases slightly up to a coverage of 0.5 corresponding to a full Na monolayer. At the minimum, where Na coverage is about 0.2, work function reduction is 0.5 eV from the full Li monolayer. At the end of a monolayer deposition, the work function is estimated to be 2.5 eV from a value of the work function of the Cu(001) surface, 4.6 eV. Reported work functions of bulk sodium and lithium metals are 2.4 and 2.9 eV, respectively. Therefore, the result of the work function is consistent with the growth mode that Na adatoms form a monolayer on the full Li monolayer preadsorbed on Cu(001).

3.3. Li on Na full monolayer

Li atoms are deposited on a full monolayer of Na atoms preadsorbed on Cu(001). Order of deposition of Li and Na is reversed in this case. The Auger spectrum of the starting surface of the full Na monolayer is depicted in Fig. 6(a). Two Na Auger peaks at 25 and 22 eV are observed, and this indicates, of course, that the Na atoms are adsorbed on the copper substrate. Figures 6(b) and (c) are Auger spectra taken after Li deposition on the Na monolayer at Li coverages of 0.24 and 1.1, respectively. Two possible growth modes are considered here: overlayer growth and substitutional growth. Suppose that the overlayer growth is the case, only the 49 eV peak of Li Auger should be observed. If the substitutional growth occurs on the other hand, both 46 and 49 eV peaks should be detected. At the same time, the 22 eV peak of Na Auger should disappear with increasing Li deposition. Now we

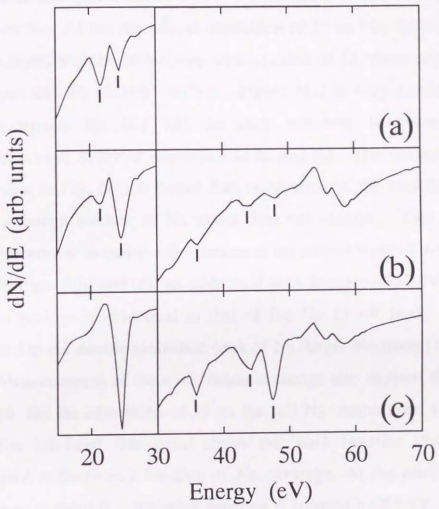

Fig. 6. The Li KVV and the Na LVV Auger electron spectra at 180 K. (a) The full Na monolayer on Cu(001), θ_{Na}=0.5. (b) Li is deposited onto the Na full monolayer, θ_{Li}=0.24. (c) same as (b) but θ_{Li}=1.1.

return to Fig. 6(c). In the spectrum two Li Auger peaks appear, whereas a single peak of 25 eV Na Auger is seen. Peak height of the 25 eV Na Auger increases with increase of Li coverage as seen in Figs. 6(a)-(c). These behaviors straightforwardly lead to a conclusion of the substitutional growth of Li on Na. At the monolayer deposition of Li on Na, the top layer consists of Na atoms and the underlying layer consists of Li atoms sandwiched by the Na layer and the Cu(001) surface. Figure 6(c) is very similar to Fig. 4(d), which reflects the fact that the same structure is formed on Cu(001) independent of order of deposition of Li and Na. The intensity of the 25 eV peak seen in Fig. 6(c) is larger than summation of the two Na peaks in Fig. 6(a), although amount of Na atoms does not change. This is an unknown phenomenon of intensity enhancement at the second layer of alkali-metals.

In Figs. 6(b) and (c), an additional peak appears at 37 eV. The intensity of this peak is proportional to that of the Na 25 eV peak. This has been assigned to the double ionization peak of Na Auger electrons [18,19].

Measurements of the work function change also support the substitutional growth for the adsorption of Li on the full Na monolayer, as shown in Fig. 7. The left-hand side panel shows the work function change of the Na deposited surfaces as a function of Na coverage. At the minimum where Na coverage is about 0.2, the work function is reduced by 2.5 eV. At the full Na monolayer the work function recovers by 0.35 eV and is estimated to be 2.45 eV. These results are similar to the literature [20]. Li atoms are deposited on the full Na monolayer and the change of the work function is plotted in the right-hand side panel of Fig. 7. It is demonstrated clearly that the work function does not change with increasing amount of Li adatoms. This suggests that Na atoms are always located in the top layer; Each Li atom substitute a Na adatom on Cu(001). In fact, the work function of the Li-monolayer deposited surface on the full Na monolayer (about 2.45 eV) is identical with that of the

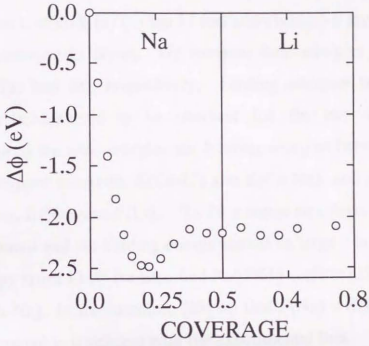

Fig. 7. Work-function change for adsorption Na on Cu(001) at 180 K with increase of Na coverage (left-hand side panel) and work-function change for adsorption of Li on the full Na monolayer on Cu(001) at 180 K as a function of Li coverage (right-hand side panel).

Na-monolayer deposited surface on the Li monolayer in the preceding section (2.5 eV).

We discuss briefly the substitutional adsorption. Here, we consider two structures on Cu(001); (a) the top Li and underlying Na layers and (b) the top Na and underlying Li layers. We compare total energies E(a) and E(b) for structures (a) and (b), respectively. Binding energies between Li and Na layers can be assumed to be identical for the two structures. Then, contribution to the total energies are binding energies between the underlying layer and copper substrate, E(Cu-Li) and E(Cu-Na), and surface energies of the top layer, E(Na) and E(Li). To be a stable structure, the surface energy should be small and the binding energy should be large. In thermal desorption spectroscopy from Li or Na adsorbed Ru(0001) surface [21,22] we find E(Ru-Li) > E(Ru-Na). In the literature [23] we find E(Na) < E(Li). Therefore, this simple argument is consistent with the experimental fact.

3.4. Na adsorption on c(2x2) structure of Li submonolayer

In this section we investigate the growth mode of Na atoms on a submonolayer of Li atoms preadsorbed on Cu(001), namely the Li-c(2x2) structure. The coverage of the Li-c(2x2) structure is 0.5, while that of the Li full monolayer is 0.8.

3.4.1. LEED *I(E)* curves

We have observed changes of LEED patterns with increase of Na deposition on the c(2x2) structure of Li atoms preadsorbed on Cu(001). The LEED patterns always exhibit c(2x2) structures up to a Na coverage of 0.5. It is found, however, that sharpness of half order spots varies with Na coverage. Initial sharp spots from the Li-c(2x2) structure on Cu(001) become broad up to Na coverage of 0.1, and finally the spots become sharp again at Na coverages larger than 0.2. This fact suggests that the c(2x2) pattern observed always during Na deposition does not come from a single structure but

originate from two structures exhibiting the same c(2x2) pattern. Here, it should be noted that both Li and Na adatoms form c(2x2) structures on Cu(001) at coverage of 0.5, as shown in Fig. 1. Therefore, we have measured *I(E)* curves of the (1/2 1/2) spot as a function of Na coverage, as shown from Fig. 8(a) to Fig. 8(f). Figure 8(a) is taken from the Li-c(2x2) structure on Cu(001) [7]. For comparison, an *I(E)* curve of the (1/2 1/2) spot of the Na-c(2x2) structure on Cu(001) is shown in Fig. 8(g) [16]. It is evident from Fig. 8 that the *I(E)* curve changes gradually from that of Li-c(2x2) to that of Na-c(2x2) with increasing Na coverage. We summarize results of LEED *I(E)* measurements as follows: (i) The Li-c(2x2) structure disappears at Na coverages between 0.1 and 0.2. (ii) The Na-c(2x2) structure is formed on Cu(001) at Na coverages larger than 0.2. Then, we propose two possible growth modes for the present adsorption system. First, substitutional growth resulting in formation of the Na-c(2x2)/Cu(001) structure covered with a disordered Li layer. We denote this as the disordered Li top-layer on Na-c(2x2)/Cu(001). Second, compression of the Li-c(2x2) structure into a disordered adlayer by Na atoms and formation of the Na-c(2x2) adlayer on vacant copper surface. In the following section, the former is excluded by the analysis of AES.

3.4.2. AES of Li KVV and Na LVV

The Auger spectra are taken after Na atom deposition on the Li-c(2x2)/Cu(001) surface as shown in Fig. 9. Coverages of Na atoms are 0, 0.25 and 0.5 for Figs. 9(a), (b) and (c), respectively. It is evident from Figs. 9(b) and (c) that two Auger peaks appear for both Li and Na atoms. This fact excludes straightforwardly the structure model of the disordered Li top-layer on Na-c(2x2)/Cu(001). The other growth model proposed above agrees with the AES result. That is, Na atoms compress the Li adlayer to become a denser monolayer, and the Na atoms do not intermix with Li adatoms and form islands of the Na-c(2x2) structure on Cu(001). The intensity ratio of the

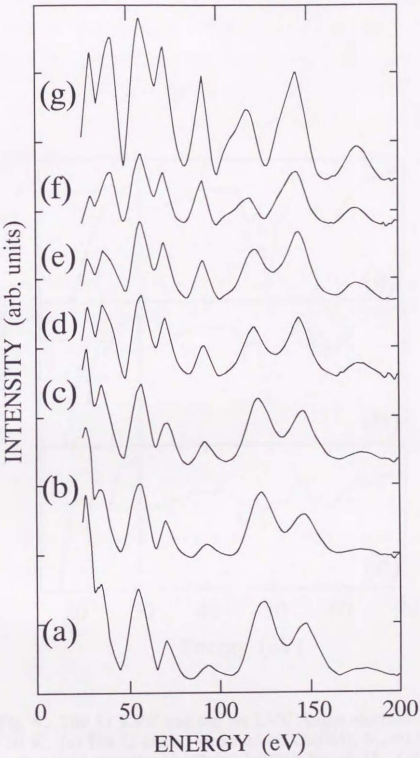

Fig. 8. *I(E)* curves for the (1/2 1/2) spot of the c(2x2) structure formed on Cu(001) at 180 K. (a) The Li-c(2x2) structure on Cu(001). (b)-(f) Na is deposited onto the Li-c(2x2)/Cu(001). θ_{Na}=0.05, θ_{Na}=0.1, θ_{Na} =0.2, θ_{Na} =0.3 and θ_{Na} =0.5 for (b)-(f), respectively. (g) The Na-c(2x2) structure on Cu(001).

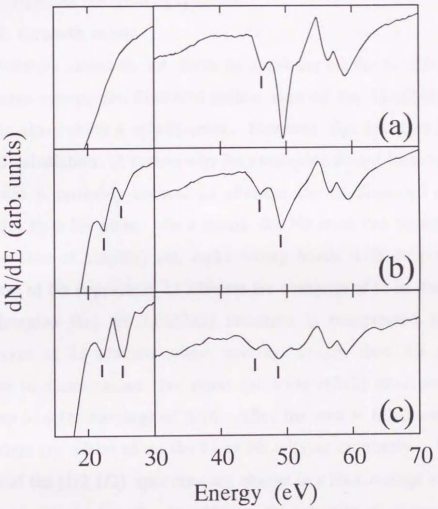

Fig. 9. The Li KVV and the Na LVV Auger electron spectra at 180 K. (a) The Li-c(2x2) structure on Cu(001), θ_{Li} =0.5. (b) Na is deposited onto the Li-c(2x2)/Cu(001), θ_{Na}=0.25. (c) same as (b) but θ_{Na}=0.5.

Na(22 eV) Auger peak to the Na (25 eV) peak in the present adsorption system seen in Fig. 9(c) is relatively smaller than that of Na adatoms on Cu(001) in Fig. 6(a). This reflects the fact that there are two kinds of Na adatoms in the coadsorption system; one adsorbs onto the Cu surface directly to form the c(2x2) structure, and the other adsorbs onto the compressed Li layer or/and on the Na-c(2x2) islands.

3.4.3. Growth mode

Why Na atoms do not form an overlayer on the Li-c(2x2)/Cu(001)? If Na atoms occupy the four-fold hollow sites of the Li-c(2x2) structure, the surface also exhibit a c(2x2) order. However, this structure is ruled out by LEED calculation. A reason why Na overlayers do not form on the Li-c(2x2) structure is probably because Li adatoms can be displaced considerably on Cu(001) by a Na atom. As a result, the Na atom can occupy the four-fold hollow sites of Cu(001) and make strong bonds with copper atoms. With increase of Na deposition, Li adatoms are compressed to be denser layers.

Imagine that the Li-c(2x2) structure is compressed into the densest overlayer of Li adatoms whose coverage is 0.8, then 3/8 of the Cu(001) surface becomes vacant. Na atoms form the c(2x2) structure on this vacant area up to a Na coverage of 3/16. After the area is filled with Na atoms up, Na atoms are adsorbed on the Li or Na adlayer randomly. In fact, the *I(E)* curve of the (1/2 1/2) spot does not change in a Na coverage range of $0.2 \leq \theta \leq 0.5$ as seen in Fig. 8. In addition, the intensity of curve (f) in Fig. 8 is smaller than that of curve (g). These results are in good agreement with that the area of the Na-c(2x2) domains is only 3/8 of the surface.

The growth mode of the present adsorption system is the compression and phase separation in a coadsorbed layer. This may be one of general phenomena for coadsorption systems. For example, a (2x2) structure of oxygen adsorbed on Pd(111) is compressed into a $(\sqrt{3}\text{x}\sqrt{3})\text{R30}^\circ$ structure with dosing CO which forms $(\sqrt{3}\text{x}\sqrt{3})\text{R30}^\circ$ domains separately [24]. At this

stage it is not clear to explain this phase separation observed in the present study, but we point out that bulk Li metal does not form alloy with Na metal [25].

4. Summary

Structure and growth of alkali-metal atoms on dissimilar alkali-metal atoms preadsorbed on Cu(001) has been studied for the first time by using AES, LEED and work function change. We have studied the following three adsorption systems at 180 K; (1) Na on a full monolayer of Li, (2) Li on a full monolayer of Na, and (3) Na on a submonolayer of Li, namely the Li-c(2x2) structure. The growth modes of these systems are summarized as follows:

(1) Na atoms form overlayers on the full Li monolayer preadsorbed on Cu(001). *(overlayer formation)*

(2) Li atoms substitute Na adatoms for adsorption of Li on the full Na monolayer preadsorbed on Cu(001). *(substitutional adsorption)*

(3) For adsorption of Na atoms on the Li-c(2x2) structure whose coverage is 5/8 of the full Li monolayer, Na atoms compress the Li adlayer to be denser monolayers. The Na atoms do not intermix with Li adatoms and form islands of the c(2x2) structure on Cu(001). *(compression and phase separation)*

To obtain these conclusions, the Li KVV and Na LVV Auger electron spectroscopies are very powerful. Appearance and disappearance of the two Auger peaks of Li and Na adatoms are examined to find growth modes. This is the first successful application of AES of the Li KVV and Na LVV transitions to surface studies.

References

[1] H.P. Bonzel, A.M. Bradshaw and G. Ertl, Eds., Physics and Chemistry of Alkali Metal Adsorption (Elsevier, Amsterdam, 1989).

[2] R.J. Behm, in Ref. 1, p. 111; C.J. Barnes, M. Lindroos, D.J. Holmes and D.A. King, in Ref. 1, p. 129.

[3] M. Okada, H. Tochihara and Y. Murata, Phys. Rev. **B 43** (1991) 1411; Surf. Sci. **245** (1991) 380.

[4] M. Okada, H. Iwai, R. Klauser and Y. Murata, J. Phys.: Condens. Matter **4** (1992) L593.

[5] H. Tochihara and S. Mizuno, Surf. Sci. **279** (1992) 89; Surf. Sci. **287/288** (1993) 423; S. Mizuno, H. Tochihara and T. Kawamura, Surf. Sci. **292** (1993) L811.

[6] C. Stampfl, M. Scheffler, H. Over, J. Burchhardt, M. Nielsen, D. L. Adams and W. Moritz, Phys. Rev. Lett. **69** (1992) 1532; C. Stampfl, J. Burchhardt, M. Nielsen, D.L. Adams, M. Scheffler, H. Over and W. Moritz, Surf. Sci. **287/288** (1993) 418; C. Stampfl, M. Scheffler, H. Over, J. Burchhardt, M. Nielsen, D.L. Adams and W. Moritz, Phys. Rev. **B49** (1994) 4959.

[7] S. Mizuno, H. Tochihara and T. Kawamura, Surf. Sci. **293** (1993) 239.

[8] T. Aruga, H. Tochihara and Y. Murata, Phys. Rev. Lett. **52** (1984) 1794; Surf. Sci. **158** (1985) 490; Surf. Sci. Lett. **175** (1986) L725; Phys. Rev. B **34** (1986) 8237.

[9] H.L. Meyerheim, J. Wever, V. Jahns, W. Moritz, P.J. Eng, I.K. Robinson, Surf. Sci. **304** (1994) 267.

[10] C. A. Papageorgopoulos, Phys. Rev. B **25** (1982) 3740.

[11] J. Cousty, R. Riwan and P. Soukiassian, Surf. Sci. **152/153** (1985) 297.

[12] S. Mizuno, H. Tochihara, T. Kadowaki, H. Minagawa, K. Hayakawa, I. Toyoshima and C. Oshima, Surf. Sci. **264** (1992) 103.

[13] S. Mizuno, H. Tochihara and T. Kawamura, J. Vac. Sci. Technol. A **12** (1994) 471.

[14] H. Tochihara and S. Mizuno, Chem. Phys. Lett., **194** (1992) 51.

[15] M.A. Van Hove and S.Y. Tong, Springer Series in Chemical Physics, Vol. 2, Surface Crystallography by LEED (Springer, Berlin, 1979).

[16] S. Mizuno,H. Tochihara and T. Kawamura, unpublished.

[17] S. Mizuno and H. Tochihara, to be published.

[18] N. Benazeth, C. Leonard, C. Benazeth, L. Viel and M. Negre, Surf. Sci., **97** (1980) 171.

[19] A.P. Janssen, R. Schoonmaker, J.A.D. Matthew and A. Chambers, Solid State Comm., **14** (1974) 1263.

[20] X. Shi, D. Tang, D. Heskett, K. -D. Tsuei, H. Ishida, Y. Morikawa and K. Terakura, Phys. Rev. **47** (1993) 4014.

[21] D.L. Doering and S. Semancik, Surf. Sci. **175** (1986) L730.

[22] D.L. Doering and S. Semancik, Surf. Sci. **179** (1986) 177.

[23] W. R. Tyson and W. A. Miller, Surf. Sci. **62** (1977) 267.

[24] T. Matsushima and H. Asada, J. Chem. Phys. **85** (1986) 1658.

[25] T. B. Murray, L. H. Bonnet and H. Baker, Binary Alloy Phase Diagram (American Society of Metals, Metals Park, OH, 1986).

VIII. Summary of the thesis

Chapter II

Surface structures of the Li/Cu(001) system are studied by LEED and AES at 180 and 300 K. At 180 K, the overlayer growth of Li adatoms is found. On the contrary, anomalous LEED patterns are observed at 300 K; 2x1, 3x3 and 4x4 with increase of the Li coverage. In the 2x1 pattern streaky spots coexist. It is found that thermal activation (about 200 K) is required for formations of these structures, and which suggests the occurrence of restructurings of substrate surfaces induced by Li adsorption. Missing-row type restructuring of Cu substrate is proposed from analysis of streaky spots and this structure is determined by LEED analysis as described in chapter V. The 3x3 and 4x4 structures are assigned to ordered surface-alloys.

Two Li KVV AES peaks are found at 49 and 46 eV, and they are assigned to Li(1s)Li(2s)Li(2s) and Li(1s)Cu(3d)Cu(3d) transitions, respectively. The latter is an interatomic transition, and the appearance of this peak suggests that Li atoms sit on Cu atoms. At 180 K, the 46 eV peak stops increasing after monolayer formation, because Li atoms in the second layer do not interact with Cu substrate. On the other hand, the 46 eV peak does not stop increasing at 300 K. This behavior leads to the conclusion that intermixing of Li and Cu occurs at 300 K. This is the first demonstration for the power of Li KVV Auger transitions, and the Li KVV Auger electron spectroscopy is succesfully used in Chapter VII..

Chapter III

We have used LEED analysis for determination of surface structures. Normal incidence condition should be satisfied in the measurement of *I(E)* curves, because the calculation of *I(E)* curves are carried at the normal incidence. Usually, a small beam-misalignment causes a fatal error to the *I(E)*

curves. Due to the small sample tilt and residual magnetic field, which are very difficult to remove, it is not easy to attain the exact normal incidence condition actually. To reduce the effects of beam-misalignment and to obtain reproduciable *I(E)* curves quickly, the horizontal-beam method is proposed. Intensities of two equivalent spots locating in the horizontal direction are measured and averaged. The guideline of the beam-alignment is described. The horizontal-beam method is succesfully used in LEED analysis described in Chapters IV and V.

Chapter IV

The first determination of surfce structures by means of LEED *I(E)* analysis is described; the c(2x2) structure formed on Cu(001) by Li deposition at 180 K. For comparison among various structural models and also for determination of bond lengths, Pendry R-factor is used. It is found that the fourfold hollow site adsorption of Li atoms at coverage of 0.5 is preferred. The Pendry R-factor is satisfactrily low, 0.106.

The results are the following;

Adsorption site: hollow-site.

Distance between Li and Cu first-layer, $d_{Li\text{-}Cu}$, is 1.96 ± 0.08 Å.

Distance between Cu first and second-layer, d_{12}, is 1.81 ± 0.04 Å.

Optimized Debye temperature of Li (T_D) is 480 K.

These results are in good agreement with recent first-principles calculation by Oguchi as follows; hollow-site is more stable, $d_{Li\text{-}Cu}$ = 1.87 Å, d_{12} = 1.80 Å, and T_D = 460 K.

Chapter V

The second determination of surface structure by LEED *I(E)* analysis is carried out for the 2x1 structure formed on Cu(001) upon Li deposition at 300 K. The following three structural models are examined; missing-row-

type restructuring of the Cu substrate, a Li overlayer on hollow-sites and a Li overlayer on on-top sites.

The results are the following;

Missing-row-type restructuring of the Cu substrate is favorable.

Distance between the first and second layers of Cu substrate, d_{12}, is 1.68 ± 0.05 Å.

Distance between the second and third layers of Cu substrate, d_{23}, is 1.84 ± 0.07 Å.

This is the first structure determination of the 2x1 structure formed on the fcc(001) surface induced by alkali-metal deposition.

Chapter VI

It is demonstrated for the first time that the slope of photoemission intensities of the substrate surface-state as a function of adsorbate coverage gives coordination number of an adsorbate atom. The surface state on Cu(001) is the Tamm-type and is observed only around $\bar{M}$ point. The intensities of the surface state are measured with increase of Li coverages at 180 and 300 K. The slopes gives the coordination number of 3 ± 1 and 6 for 180 and 300 K, respectively. These numberes are in good agreement with the surface structures determined by LEED *I(E)* analysis described in Chapter IV and V.

Chapter VII

Deposition of alkali-metal atoms on dissimilar alkali-metal monolayers preadsorbed on Cu(001) is studied for the first time by LEED, AES and work-function change. By using AES of Li KVV and Na LVV, it is possible to distinguish whether the alkali-metal atoms sitting on the Cu substrate or locating on the alkali-metal atoms. It is found that the simple overlayer formation of Na takes place on the full Li monolayer while Li atoms substitute

Na adatoms for Li adsorption on the full Na monolayer. For adsorption of Na on the Li-c(2x2) structure whose coverage is 5/8 of the saturation coverage, it is found that the Na atoms compress the Li adlayer to become denser monolayer. The Na atoms do not intermix with Li adatoms and form islands of the c(2x2) structre.

We have observed various types of displacements of substrate and adsorbate atoms induced by alkali-metal deposition. These displacements were studied by using LEED analysis, ARUPS and interatomic Auger transitions of alkali-metal atoms. I would like to note that displacements of substrate or/and adsorbate atoms might play a significant role in various surface processes and phenomena such as diffusion, ordering, phase transition, surface materials formation, catalysis and so on.

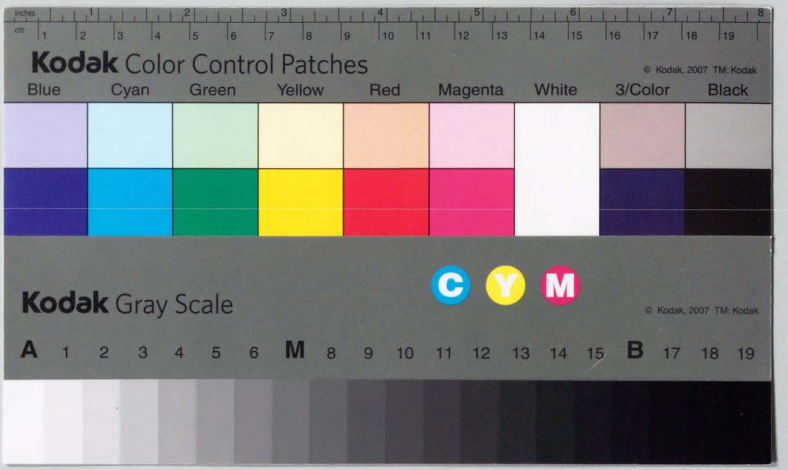
inches
cm
Kodak Color Control Patches
© Kodak, 2007 TM: Kodak
Blue
Cyan
Green
Yellow
Red
Magenta
White
3/Color
Black
Kodak Gray Scale
C
Y
M
© Kodak, 2007 TM: Kodak
A 1 2 3 4 5 6 M 8 9 10 11 12 13 14 15 B 17 18 19